ANALYSIS OF THE ELECTROMAGNETIC FIELD INSIDE THE GRADIENT COILS AND INVESTIGATION OF THE NERVE AND CARDIAC STIMULATION RISK FOR THE PATIENTS DURING MRI

A THESIS

SUBMITTED TO THE DEPARTMENT OF ELECTRICAL AND

ELECTRONICS ENGINEERING

AND THE INSTITUTE OF ENGINEERING AND SCIENCES

OF BILKENT UNIVERSITY

IN PARTIAL FULFILLMENT OF THE REQUIREMENTS

FOR THE DEGREE OF

MASTER OF SCIENCE

By

Esra Abacı

July 2008

I certify that I have read this thesis and that in my opinion it is fully adequate, in scope and in quality, as a thesis for the degree of Master of Science.

Prof. Dr. Ergin Atalar(Supervisor)

I certify that I have read this thesis and that in my opinion it is fully adequate, in scope and in quality, as a thesis for the degree of Master of Science.

Assoc. Prof. Dr. Vakur B. Ertürk

I certify that I have read this thesis and that in my opinion it is fully adequate, in scope and in quality, as a thesis for the degree of Master of Science.

Prof. Dr. Nevzat G. Gençer

Approved for the Institute of Engineering and Sciences:

Prof. Dr. Mehmet Baray
Director of Institute of Engineering and Sciences

ABSTRACT

ANALYSIS OF THE ELECTROMAGNETIC FIELD INSIDE THE GRADIENT COILS AND INVESTIGATION OF THE NERVE AND CARDIAC STIMULATION RISK FOR THE PATIENTS DURING MRI

Esra Abacı
M.S. in Electrical and Electronics Engineering
Supervisor: Prof. Dr. Ergin Atalar
July 2008

During magnetic resonance imaging (MRI), the static magnetic field, the radio frequency field and the gradient fields are utilized. In the literature, there are several studies with the aim of understanding the bioeffects of these fields. Due to the time varying gradient fields, an electric field is induced in the body which may cause nerve and cardiac stimulation. In order to investigate this risk, researchers have been working on solving the induced electric field both analytically and by using computational methods. The field distribution inside the body has also been investigated. It is vital to verify the risk of MRI to patients with an implant. In order to improve the understandability of the field pattern, the field should be expressed as simple as possible.

In this thesis, the simplified expressions of induced electric field are derived inside and outside of the cylindrical, homogenous volume, which is taken as the human body model. For this derivation, low frequency based assumptions are used and

gradient field is assumed to be perfectly uniform. The obtained results satisfy the expected conditions for the electric and magnetic fields. The field patterns obtained with these simplified expressions are compared with the former studies and the maximum electric field values obtained for a different gradient field and slew rates are used to investigate the stimulation risk. Moreover, by using these electric field values, the worst position for an implant lead and the length of the lead is determined.

We believe that with these simplified expressions, the understandability of the field distribution is enhanced and to comment on the risk of MRI to a patient with an implant becomes easier.

Keywords: MRI, Gradient Coils, Electric Field, Stimulation, Implant

ÖZET

MR GÖRÜNTÜLEME SIRASINDA GRADYAN SARGILAR İÇİNDE OLUŞAN ELEKTROMANYETİK ALANIN ANALİZİ VE HASTADA GÖRÜLEBİLECEK KALP VE SİNİR UYARIMI RİSKİNİN İNCELENMESİ

Esra Abacı
Elektrik ve Elektronik Mühendisliği Bölümü Yüksek Lisans
Tez Yöneticisi: Prof. Dr. Ergin Atalar
Temmuz 2008

Manyetik Rezonans Görüntüleme süresince, ortamda sabit manyetik alan, radyofrekans alanı ve gradyan manyetik alan oluşur. Oluşan bu alanların biyolojik etkilerinin anlaşılması için bir çok çalışma yapılmıştır. Zamana bağlı değişen gradyan manyetik alan, görüntülenen vücut içinde elektrik alan indükler. İndüklenen elektrik alan sinir ve kalp uyarımına sebep olur. Bu riskin anlaşılması için, indüklenen elektrik alan matamatiksel olarak ve bilgisayar destekli hesaplama yöntemleriyle çözülmeye ve alan dağılımı anlaşılmaya çalışılmıştır. Bu, aynı zamanda vücuduna üreteç yerleştirilmiş hastaların MR ile görüntülenmelerinin oluşturabileceği riskin anlaşılması için de önemlidir. Alan dağılımının kolaylıkla anlaşılabilmesi için, denklemler basitleştirilmelidir.

Bu tezde, homojen iletkenliğe sahip silindirik bir hacim olarak modellenmiş vücut içinde ve dışında indüklenen elektrik alan denklemi basitleştirilmiştir. Basitleştirilmiş denklemlere ulaşmak için, düşük frekans yaklaşımı kullanılmıştır ve gradyan sargının ürettiği alanın tamamen bir örnek dağılıma sahip olduğu kabul

edilmiştir. Elde edilen manyetik ve elektrik alan denklemleri gerekli matematiksel durumları sağlamaktadır. Bu denklemlerle alan dağılımları oluşturulmuş ve daha önceki çalışmaların sonuçlarıyla karşılaştırılmıştır. Farklı sargı modelleri için en yüksek elektrik alan değerleri bulunmuş; bu değerler üreteç kablosunun vücutta yerleştirilebilecek en riskli yerinin tespiti ve kablonun uzunluğunun belirlenmesi için kullanılmıştır.

Basitleştirilmiş elektrik ve manyetik alan denklemleriyle, alan dağılımın anlaşılabilirliğini ve üreteç taşıyan hastaların MR içinde maruz kalabileceği riskin yorumlanmasını kolaylaştırdığımıza inanıyoruz.

Anahtar Kelimeler: MR Görüntüleme, Gradyan Sargılar, Elektrik Alan, Stimülasyon, Üreteç

ACKNOWLEDGMENTS

I wish to express my deepest regards to my supervisor Prof. Dr. Ergin Atalar. Conducting research with Dr. Atalar has been a great chance for me. He shares his knowledge and experience with his students and motivates us. He is a perfect model both as a person and as an academician for me. Moreover, working with his biomedical group has been a great experience for me. I have to thank all the group members.

I would like to thank to Dr. Vakur B. Ertürk and Prof. Dr. Ayhan Altıntaş for their valuable discussions throughout my M.S. study.

I would also like to thank to my officemate and colleague Emre Kopanoğlu for his help during my thesis. My special thanks go to my dear friends Hakan, Ezgi, Figen, Gülis, Elif, Kıvanç, Bora, Kağan and my dear sibling Gökçen. Without them I would have already ran away.

My special thanks go to my big-hearted family. Without their love and confidence to me, I could not manage to finish this study.

Last but not least, I would like to thank to Ata Türk for coming into my life at the right time.

This work was partially supported by TUBITAK 1001 grant 107E108 and the TUBITAK fellowship, 2228 for M.Sc. studies.

Contents

List of Figures

List of Tables

To my family ...

Chapter 1

INTRODUCTION

1.1 Motivation and Literature Survey

The magnetic resonance imaging (MRI) is a widely used diagnostic technique. Since the introduction of MRI in the clinical platform in the early 1980s, more than 100,000,000 diagnostic procedures have been completed in the world [4]. MRI scanners need static magnetic field as well as radio-frequency and gradient magnetic fields in order to obtain images. Due to these fields, MR environment and MRI scanning have the potential to induce hazardous effects to the patient. These MR-related injuries are generally because of the metallic objects which are not compatible to the MR environment. Moreover, the patients with implants or devices are under the risk of excessive heating or nerve stimulation due to the induction of the current [4]. Neuro-stimulation systems and cardiac pacemakers are generally used active implantable medical devices (AIMD). In the world, it is estimated that more than 2 million patients have cardiac pacemakers [5]. Patients with cardiac pacemakers generally need MR scanning, since MRI has been applied successfully to monitor myocardial wall motion and perfusion. As a result, cardiac pacemakers are the most common implant which have been tested

for MR safety or MR compatibility [5].

The static magnetic field is the key component of MRI, because the magnetization of the hydrogen nuclei in the human water molecules align with this strong magnetic field. In order to understand the bioeffects of the static magnetic field, many studies have been performed, and, at the end, majority of these studies state that there is no verified substantial harmful bioeffect [6]. Although potentially harmful effects of static magnetic field on isolated cells or organisms are observed, there is no documented scientific fact. One of the biological effect is magnetohydrodynamics which causes the change in blood viscosity. But this effect is not significant below 10 T [7]. Generally, the serious injuries due to the static field are because of the ferromagnetic objects around the MR [8]. Due to the static field, forces induced on magnetic components tend to align these objects' long axis along the field, which causes the movement of the implants inside the body [9].

In MRI scanners, the radio frequency (RF) field is required in order to induce precession in the nuclei of concern. The bioeffects of RF field are related with the heating [8]. For patients with AIMD, the risk increases due to hazardous RF heating at the lead tips of the implants. In order to understand the parameters affecting the heating, and to determine the worst position of the implant that may cause the burning of the tissue, various experimental studies are performed [10, 11].

The gradient fields are required to select the slice, to vary the phase distributions of the excited spins and also to spatially vary the frequency of the spins. By utilizing the signal data obtained with the help of the gradient fields, the

image of the selected slice can be reconstructed via Fourier transformation techniques. There are three independent gradient coils, which are called as x, y, and z-gradient coils. For imaging purposes, the magnetic field is defined in the z direction. An ideal gradient field is given as $B_z = G_x x + G_y y + G_z z$. Although non-uniformity in the gradient field causes undesired effects such as image distortion, it is not possible to obtain a perfectly uniform gradient magnetic field [12]. Gradient waveforms are usually designed as pulses. The ramp up and down times are usually considered as dead times and they need to be minimized for maximum performance. During MRI, this rapidly switched gradient magnetic field induces an electric field and the magnitude of this field is proportional with the rate of change of the magnetic field.

Since the human nervous system is sensitive to the field variations at low frequencies [13], an induced electric field may cause nerve stimulation. To investigate the stimulation risk and the threshold value, many experimental studies have been carried out [14–19]. Furthermore, in order to define the induced electric field that causes stimulation, both computational methods such as finite difference time domain method, and analytical calculations have been performed in the literature by using inhomogeneous and homogenous human models [1,20,21]. Although the results of these studies give the general behavior of the field patterns graphically, a simple analytical expression that gives the safety threshold does not exist.

The effect of the time varying magnetic field to the implant inside the body is an important safety problem [2, 22]. In one report, due to gradient field, asynchronous pacing of a patient with an implanted pacemaker was observed [23]. In order to understand this effect fully, the gradient induced current on an implant should be investigated. The model for the induction of the gradient induced

current is given in [9]. However, in order to obtain a simple formula for the induced current, first, the field distribution should be calculated and observed explicitly. The main goal of the simplification of the expressions is to investigate the interaction of an implant and the gradient field more easily and to obtain the simple model describing the stimulation risk.

The subject of this study is to investigate the safety concerns related with the gradient magnetic fields. This study starts with the analysis of the behavior of the field distribution inside the body. The gradient coil design procedures are investigated to understand the behavior of the gradient field. Under the low frequency based assumptions, for a cylindrical, homogenous human body model, simple analytic expressions of the electric and magnetic fields are obtained. By using these simplified expressions, the worst position and length of the implants causing stimulation are defined. The maximum length of the straight part of the pacemaker lead is also determined.

1.2 The Objective and Scope of the Thesis

In this thesis, the gradient coils and the gradient field in magnetic resonance imaging scanners are investigated. The analytical calculations and simplification of the expressions are performed for the electric and magnetic field, which occur due to this time varying gradient field. Using these simplified expressions, field patterns are obtained for the safety of the patient. The worst case scenarios causing stimulation for the patients with and without an implant are analyzed. The risk for the patients with a pacemaker is also investigated.

The thesis is divided into chapters, Chapter 1 introduces the subject and gives the motivation behind this study. Chapter 2 gives the general information about

the gradient coil design procedure and the gradient field. In Chapter 3, analytical calculations of the electric and magnetic field and simplification steps of these expressions are introduced. Moreover, in this chapter, obtained field patterns with these simplified expressions are given. Chapter 4 presents the safety concern of the gradient field. At the end, Chapter 5 includes the discussions, conclusions and future work. Appendices A and B contain additional simplification steps of the fields, produced by y and z-gradient coils.

Chapter 2

GRADIENT COILS

2.1 Magnetic Field Distribution in Gradient Coil

Three spatially independent and time controllable gradient fields are produced by gradient coils. Their magnitudes are significantly smaller than the magnitude of the main field and in the order of millitesla per meter (mT/m) [24]. Quality and uniformity of the MR image over the volume of interest (VOI) are directly related to the strength and linearity of the gradient field over the imaging volume [25]. Spatial non-linearity of the gradient field causes image distortions. The non-linear gradient field is the reason of the excitation of the undesired nuclei outside the slice. The receiver detects resonance signals from different positions and all these signals are used in the reconstruction process [24]. Moreover, in order to use a simple reconstruction algorithm, like 3D-Fourier transformation, a linear characteristic of the field in space is needed [25]. The variation of the gradients G_x, G_y and G_z shows the linearity of the gradient fields [26]. For imaging purposes, only the z-component of the gradient magnetic field is important [25].

For each coordinate, there is one coil system. In order to understand the electromagnetic field distribution, first, the total magnetic field should be formulated. As the design parameter, the z-component of the magnetic field is given as $B_z = G_x x + G_y y + G_z z$. Bernstein et al. [27] have done a similar work earlier. For the sake of completeness, the formulation steps are described below.

It is well-known that a linear function can be expressed as $f(x) = x\frac{df}{dx}$. Similarly a perfectly linear field can be expressed as:

$$\vec{B} = (\vec{r} \cdot \nabla)\vec{B}. \tag{2.1}$$

The relationship between the magnetic field components in the matrix form is:

$$\begin{bmatrix} B_x \\ B_y \\ B_z \end{bmatrix} = \begin{bmatrix} \frac{\partial B_x}{\partial x} & \frac{\partial B_x}{\partial y} & \frac{\partial B_x}{\partial z} \\ \frac{\partial B_y}{\partial x} & \frac{\partial B_y}{\partial y} & \frac{\partial B_y}{\partial z} \\ \frac{\partial B_z}{\partial x} & \frac{\partial B_z}{\partial y} & \frac{\partial B_z}{\partial z} \end{bmatrix} \begin{bmatrix} x \\ y \\ z \end{bmatrix} = \begin{bmatrix} \frac{\partial B_x}{\partial x} & \frac{\partial B_x}{\partial y} & \frac{\partial B_x}{\partial z} \\ \frac{\partial B_y}{\partial x} & \frac{\partial B_y}{\partial y} & \frac{\partial B_y}{\partial z} \\ G_x & G_y & G_z \end{bmatrix} \begin{bmatrix} x \\ y \\ z \end{bmatrix}, \tag{2.2}$$

where $\frac{\partial B_z}{\partial x} = G_x$, $\frac{\partial B_z}{\partial y} = G_y$ and $\frac{\partial B_z}{\partial z} = G_z$.

In Maxwell equations, relation between the current and magnetic field is defined as $\nabla \times \vec{B} = \mu_0(\vec{J} + \sigma\vec{E} + \frac{\partial \epsilon \vec{E}}{\partial t})$, where $\vec{J}$ is the source current. Under low frequencies, due to large skin depth, induced current can be ignored, and due to small permittivity range, displacement current can also be ignored. The source current density $\vec{J}$ inside the imaging volume is zero. So, within the imaging volume, B-field expression has a curl free nature, i.e., $\nabla \times \vec{B} = 0$ (Note that, on the gradient coil, due to current on the wires, it is non-zero.).

$$\nabla \times \vec{B} = \hat{x}\{\frac{\partial B_z}{\partial y} - \frac{\partial B_y}{\partial z}\} - \hat{y}\{\frac{\partial B_z}{\partial x} - \frac{\partial B_x}{\partial z}\} + \hat{z}\{\frac{\partial B_y}{\partial x} - \frac{\partial B_x}{\partial y}\} = 0 \tag{2.3}$$

In addition, divergence of magnetic field has to be zero, i.e., $\nabla \cdot \vec{B} = 0$.

$$\nabla \cdot \vec{B} = \frac{\partial B_x}{\partial x} + \frac{\partial B_y}{\partial y} + \frac{\partial B_z}{\partial z} = \frac{\partial B_x}{\partial x} + \frac{\partial B_y}{\partial y} + G_z = 0, \tag{2.4}$$

where $\hat{x}$, $\hat{y}$, $\hat{z}$ are unit vectors in x, y and z directions, respectively.

From Eq.(2.3) and Eq.(2.4), each partial derivative components can be expressed as:

$$\frac{\partial B_y}{\partial z} = \frac{\partial B_z}{\partial y} = G_y, \tag{2.5}$$

$$\frac{\partial B_x}{\partial z} = \frac{\partial B_z}{\partial x} = G_x, \tag{2.6}$$

$$\frac{\partial B_y}{\partial x} = \frac{\partial B_x}{\partial y} \equiv g, \tag{2.7}$$

$$\frac{\partial B_x}{\partial x} + \frac{\partial B_y}{\partial y} = -G_z. \tag{2.8}$$

As mentioned in the study [27], for a coil with cylindrical symmetry partial derivatives ($\frac{\partial B_x}{\partial x}$) and ($\frac{\partial B_y}{\partial y}$) are equal to each other and to $-0.5G_z$ according to Eq.(2.8). The derivatives ($\frac{\partial B_y}{\partial x}$) and ($\frac{\partial B_x}{\partial y}$) are equal to each other and for a linear field they are also equal to a constant, g. Since these are not the desired gradients their equivalents, g, can be taken as zero in Eq.(2.7) for imaging purposes. As a result, each partial derivative in Eq.(2.2) can be expressed as:

$$\begin{bmatrix} B_x \\ B_y \\ B_z \end{bmatrix} = \begin{bmatrix} -0.5G_z & 0 & G_x \\ 0 & -0.5G_z & G_y \\ G_x & G_y & G_z \end{bmatrix} \begin{bmatrix} x \\ y \\ z \end{bmatrix}. \tag{2.9}$$

Then, for perfectly uniform gradient field the total magnetic field expression in cartesian coordinates for x, y, and z-coils, can be given as the following:

$$\vec{B} = G_x(z\hat{x} + x\hat{z}) + G_y(z\hat{y} + y\hat{z}) + G_z(-0.5x\hat{x} - 0.5y\hat{y} + z\hat{z}). \tag{2.10}$$

2.2 Design of Gradient Coil

Linearity of the gradient over a large volume of interest, short switching time (i.e., low inductance), low power consumption and high current efficiency (the ratio of the generated gradient field to the current drawn) are the important aspects that should be taken into consideration in the design of a gradient coil [26].

To find the optimal position of the multiple windings of coils, there are a number of approaches such as matrix inversion technique [28], stream function method [29], and target field approach [30]. Generally, with these methods, a continuous current density on a coil former is derived and this current is converted to a pattern of discrete current paths to design a gradient coil [28].

In this thesis, in order to understand the field distribution inside the gradient coil, first, the current distribution and the magnetic field are investigated by using the target field method [30]. In the target field method, Ampere's law is used to calculate the required currents directly from the specification of the desired field. First, the current density, $\vec{J}_{coil}$ flowing through a simple geometry, is used as the source of the magnetic field [28]. Then, the gradient target field is defined as $B_z(\rho, \phi, z) = g(z)f(\rho, \phi)$ where $g(z)$ gives a specified variation with respect to z and $f(\rho, \phi)$ describes the azimuthal and radial variation of B_z [30]. According to Turner [30], $g(z)$ function can have a form of $g(z) = [1 + (\frac{z}{d})^6]^{-1}$, where d is a constant. For perfectly uniform gradients, $g(z)$ is taken as unity. In this thesis in order to solve the electromagnetic field expressions analytically, $g(z) = 1$ is used. Note that, in order to obtain such a linear field, an infinitely long gradient coil is required.

In the next chapter, the electromagnetic field is calculated by using the target field method, and the resultant magnetic field expression is compared with Eq.(2.10).

Chapter 3

THE ELECTRIC FIELD INDUCED BY TIME VARYING GRADIENT FIELDS

3.1 Analytical Calculations of the Electric Field

To understand the risk of the stimulation due to gradient fields, first, the induced electric field distribution should be defined as mentioned before. The electric and magnetic field expressions derived for cylindrical homogenous body model by Bowtell and Bowley [1] provide a general understanding of the field distribution inside the body. These electric and magnetic field expressions for the current passing through the coils are in the form of a Fourier Transform and a Fourier integral. Thus, for a given current in a cylindrical gradient coil, electric and magnetic field patterns can only be observed after evaluating this transform and integral numerically. However, this process might be challenging for certain current distributions. On the other hand, without such a computational work, it is difficult to understand these field distributions. In this thesis, apart from the

expressions derived for the electromagnetic fields inside of the body, the expression describing the electric field outside of the body is also derived. As a body model, an infinitely long, cylindrical, homogenous volume with the conductivity, σ, and the radius, ρ_0, is used. All derived expressions are simplified and presented in short, analytical forms (closed-form expressions) for a perfectly linear gradient field formed by an infinitely long gradient coil.[1] In the region which includes the uniform field distribution, stimulation risk can easily be defined with these simplified expressions.

3.1.1 Theory

In the study [1], to calculate the electric field, first the scalar potential V, and the vector potential $\vec{A}$, are evaluated inside the gradient coil. $\vec{A}$ is the magnetic vector potential due to currents in gradient coils and V is due to the electric charge at the interface of discontinuities in electrical conductivity and conservation of electric charge. Maxwell's equations are:

$$\nabla \times \vec{B} = \mu_0(\vec{J} + \frac{\partial \vec{D}}{\partial t}), \tag{3.1}$$

$$\nabla \cdot \vec{B} = 0, \tag{3.2}$$

$$\nabla \times \vec{E} = -\frac{\partial \vec{B}}{\partial t}, \tag{3.3}$$

$$\nabla \cdot \vec{D} = \rho_f(\vec{r}, t), \tag{3.4}$$

where $\rho_f(\vec{r})$ is the charge density, $\vec{J}$ is the current density, μ_0 is the permeability of free space, and $\vec{D} = \epsilon\vec{E}$ is the current displacement with the permittivity ϵ, and $\vec{r}$ is the position vector. The current density is defined as $\vec{J} = \vec{J}^{coil} + \sigma\vec{E}$, where $\vec{J}^{coil}$ is the density of the current passing through the coil. Magnetic field $\vec{B}$, and electric field $\vec{E}$, can be expressed in terms of the scalar potential, and the

[1]This work has been also presented in ISMRM'08 at Toronto. E. Abacı, E. Kopanoğlu,V. B. Ertürk, E.Atalar,"Simple Analytical Equation of the Induced E-Field", ISMRM 16^{th} annual meeting, Toronto, May 2008

vector potential as:

$$\vec{B} = \nabla \times \vec{A}(\vec{r}, t), \tag{3.5}$$

and

$$\vec{E} = -\nabla V(\vec{r}, t) - \frac{\partial \vec{A}(\vec{r}, t)}{\partial t}. \tag{3.6}$$

Quasi-Static Limit

For gradient waveforms, frequency level is smaller than 10 kHz. Conductivity of the volume is assumed to be uniform and nearly equal to the average of the conductivity of tissues inside the body [31]. Under these conductivity and low frequency based assumptions, skin depth ($\delta = (\frac{2}{\omega\mu\sigma})^{\frac{1}{2}}$) is much larger than the physical size of the stimulated tissue region which means that the induced current inside the body is not a source to generate magnetic field. In other words, this induced current inside the body does not contribute to the vector potential.

The permittivity of biological tissues varies between 10^{-7} F/m and 10^{-5} F/m for a frequency range from 10 Hz to 10 kHz. The ratio of the displacement to the conduction current is of order $\frac{\omega\epsilon}{\sigma}$ and this is much smaller than 1. Based on this knowledge, the displacement current can be ignored (i.e., $\frac{\partial \vec{D}}{\partial t} \rightarrow 0$).

Under these low frequency based assumptions the scalar and vector potential equations can be simplified. First, wave equation for vector potential is described. By using the Eq.(3.5) in the Eq.(3.1), the wave equation is found after the following steps:

$$\nabla \times \nabla \times \vec{A} = \mu_0(\vec{J}^{coil} + \sigma\vec{E} + \frac{\partial \vec{D}}{\partial t}), \tag{3.7}$$

$$\nabla(\nabla \cdot \vec{A}) - \nabla^2\vec{A}(\vec{r}, t) = \mu_0\vec{J}^{coil} + \mu_0(\sigma + \epsilon\frac{\partial}{\partial t})\vec{E}, \tag{3.8}$$

where $\vec{E} = -\nabla V(\vec{r}, t) - \frac{\partial \vec{A}(\vec{r}, t)}{\partial t}$, by inserting this to the wave equation:

$$\nabla(\nabla \cdot \vec{A}) - \nabla^2\vec{A}(\vec{r}, t) = \mu_0\vec{J}^{coil} - \nabla(\mu_0\sigma V) - \mu_0\sigma\frac{\partial \vec{A}}{\partial t}$$

$$- \quad \nabla(\mu_0\epsilon\frac{\partial V}{\partial t}) - \mu_0\epsilon\frac{\partial^2\vec{A}}{\partial t^2}, \tag{3.9}$$

$$\nabla(\underbrace{\nabla\cdot\vec{A} + (\mu_0\sigma + \mu_0\epsilon\frac{\partial}{\partial t})}_{0}V - \nabla^2\vec{A}(\vec{r},t) = \mu_0\vec{J}^{coil}\underbrace{-\mu_0\sigma\frac{\partial\vec{A}}{\partial t} - \mu_0\epsilon\frac{\partial^2\vec{A}}{\partial t^2}}_{0} \tag{3.10}$$

Due to Lorentz gauge, $\nabla\cdot\vec{A} + (\mu_0\sigma + \mu_0\epsilon\frac{\partial}{\partial t})V = 0$ is used and also $-\mu_0\sigma\frac{\partial\vec{A}}{\partial t} - \mu_0\epsilon\frac{\partial^2\vec{A}}{\partial t^2} \approx 0$. Since, this part is reorganized in phasor domain such that:

$$(-i\mu_0\sigma\omega + \mu_0\epsilon\omega^2)\vec{A} = \underbrace{\mu_0\sigma\omega}_{=\frac{2}{\delta^2}}(-i + \frac{\omega\epsilon}{\sigma})\vec{A}, \tag{3.11}$$

where δ is the skin depth, and for large skin depth as mentioned before for quasi-static case, this part is ignored [32].

So, the resultant vector potential relation becomes:

$$\nabla^2\vec{A}(\vec{r},t) = -\mu_0\vec{J}^{coil}(\vec{r},t). \tag{3.12}$$

For scalar potential Eq.(3.6) is used in Eq.(3.4):

$$\nabla\cdot(-\nabla V - \frac{\partial\vec{A}}{\partial t}) = \frac{\rho_f}{\epsilon}. \tag{3.13}$$

In the Lorentz gauge, again due to low conductivity and permittivity values, $\nabla\cdot\vec{A}$ can be taken as approximately zero. So, resultant scalar potential relation becomes:

$$\nabla^2 V(\vec{r},t) = -\frac{\rho_f}{\epsilon}. \tag{3.14}$$

Moreover, to solve the scalar and vector potential equations, an appropriate boundary condition on the surface of the cylindrical volume is applied. It is known that divergence of Eq.(3.1) should be zero, so $\nabla\cdot(\vec{J} + \frac{\partial\vec{D}}{\partial t}) = 0$ and also because of the quasi-static assumption $\frac{\partial\vec{D}}{\partial t} = 0$, the relationship $\nabla\cdot\vec{J} = 0$ is obtained. This expression means that any component of the current normal to surface should be continuous. Inside the body there is conductivity σ, hence the current can be defined as $\vec{J} = \sigma\vec{E}$, whereas conductivity is zero outside of the body, and thus the current is zero. For a cylindrical surface ρ component of the

current is normal to the surface, so it should be continuous. In order to see this continuity at the surface, ρ component of the electric field at the boundary should also be zero due to zero current at the outside (i.e., at the boundary $E_\rho = 0$).

Note that any complicated waveform can be expressed as the combination of each frequency component. Therefore, using this fact, Bowtell [1] has used sinusoidal waveforms for the fields (i.e., $\vec{J}^{coil}(\vec{r},t) = Re\{\vec{J}^{coil}(\vec{r})e^{i\omega t}\}$). The following expressions in this chapter are in the phasor domain.

Scalar potential equations

Under the low frequency based assumptions, it is also assumed that in the bulk of the body there is no charge, so thus the Laplace's equation, $\nabla^2 V = 0$ can be solved. Solution of the Laplace's equation in cylindrical coordinates is in the form of [26]:

$$V(\rho,\phi,z) = \frac{1}{2\pi}\sum_{m=-\infty}^{\infty} e^{im\phi}\int_{-\infty}^{\infty} e^{ikz}V^m(k,\rho)dk, \tag{3.15}$$

where k is the spatial frequency.

Laplace's equation can be explicitly written as:

$$\frac{1}{\rho}\frac{\partial}{\partial\rho}(\rho\frac{\partial V}{\partial\rho}) + \frac{1}{\rho^2}\frac{\partial^2 V}{\partial\phi^2} + \frac{\partial^2 V}{\partial z^2} = 0. \tag{3.16}$$

By using the knowledge that the basis functions of Fourier Series expansion, $e^{im\phi}$, form an orthogonal set, the operations such as summation and differentiation with respect to space can be performed only on the expansion coefficients of corresponding fields. As a result, the relation for $V^m(k,\rho)$ becomes:

$$\frac{1}{\rho}\frac{\partial}{\partial\rho}(\rho\frac{\partial V^m}{\partial\rho}) - \frac{m^2}{\rho^2}V^m - k^2V^m = 0. \tag{3.17}$$

By multiplying both sides of the Eq.(3.17) with " ρ^2 " [26], the expression becomes:

$$\rho\frac{\partial}{\partial\rho}(\rho\frac{\partial V^m}{\partial\rho}) - k^2\rho^2V^m - m^2V^m = 0. \tag{3.18}$$

General solution of Eq.(3.18) is given by $V_m = aI_m(k\rho) + bK_m(k\rho)$ [26], where a and b are constants and $I_m(k\rho)$ and $K_m(k\rho)$ are first and second kind modified Bessel functions of order m, respectively. Two of the basic properties of these Bessel functions are [26]:

$$I_m(k\rho) \to \infty \; as \; \rho \to \infty, \tag{3.19}$$

$$K_m(k\rho) \to \infty \; as \; \rho \to 0. \tag{3.20}$$

Since the scalar potential must be finite both at the origin and infinity, according to Eq.(3.19) and Eq.(3.20), inside the body, the constants become $a = \alpha_m$ and $b = 0$ and outside the body, they are $a = 0$ and $b = \beta_m$, so the general solution for scalar potential component is:

$$for \; \rho < \rho_0 \quad V^m(k,\rho) \;\; = \;\; \alpha_m(k)I_m(k\rho), \tag{3.21}$$

$$for \; \rho > \rho_0 \quad V^m(k,\rho) \;\; = \;\; \beta_m(k)K_m(k\rho). \tag{3.22}$$

In order to find the constants α_m and β_m, the boundary condition at the surface of the body is used (i.e., $E_\rho(\rho = \rho_0) = 0$) in the Eq.(3.6). Before the analysis of this equation, first the analytical form of the magnetic field B, electric field E and vector potential should be defined similar to the scalar potential such as:

$$U_c(\rho,\phi,z) = \frac{1}{2\pi}\sum_{m=-\infty}^{\infty} e^{im\phi}\int_{-\infty}^{\infty} e^{ikz}U_c^m(k,\rho)dk, \tag{3.23}$$

where U describes B, E or A and c can be ρ, ϕ or z.

With this form of the fields, by using similar reasoning in Eq.(3.17) about the orthogonality Eq.(3.6) is written as:

$$E_\rho^m = -\frac{\partial V^m}{\partial\rho} - i\omega A_\rho^m. \tag{3.24}$$

Then, this equation is solved at the boundary to find the constants of the scalar potential.

While approaching to the boundary, $\rho = \rho_0$ from inside, Eq.(3.21) is used in the Eq.(3.24) and the resultant relation is:

$$E_\rho^m = -\frac{\partial(\alpha_m(k) I_m(k\rho))}{\partial\rho} - i\omega A_\rho^m \;=\; 0 \; at \; \rho = \rho_0, \tag{3.25}$$

$$-k\alpha_m(k) I'_m(k\rho_0) - i\omega A_\rho^m(k,\rho_0) \;=\; 0, \tag{3.26}$$

where $I'_m(k\rho)$ is the derivative of the first order modified Bessel function with respect to its variable (i.e., $I'_m(x) = \frac{dI_m(x)}{dx}$). Moreover, the scalar potential should be continuous at the surface in order to satisfy the continuity of the ρ component of the electric field at the boundary. Therefore:

$$\alpha_m(k) I_m(k\rho_0) = \beta_m(k) K_m(k\rho_0). \tag{3.27}$$

As a result, constants become:

$$\alpha_m(k) \;=\; -\frac{i\omega A_\rho^m(k,\rho_0)}{k I'_m(k\rho_0)}, \tag{3.28}$$

$$\beta_m(k) \;=\; -\frac{i\omega A_\rho^m(k,\rho_0) I_m(k\rho_0)}{k I'_m(k\rho_0) K_m(k\rho_0)}. \tag{3.29}$$

With these constants the solution for the components of the scalar potential becomes:

$$for \; \rho < \rho_0 \;\; V^m(k,\rho) \;=\; -\frac{i\omega A_\rho^m(k,\rho_0) I_m(k\rho)}{k I'_m(k\rho_0)}, \tag{3.30}$$

$$for \; \rho > \rho_0 \;\; V^m(k,\rho) \;=\; -\frac{i\omega A_\rho^m(k,\rho_0) I_m(k\rho_0) K_m(k\rho)}{k I'_m(k\rho_0) K_m(k\rho_0)}. \tag{3.31}$$

In terms of scalar and vector potential components, each component of the electric field for $\rho < \rho_0$ can be written as:

$$\begin{aligned} E_\rho^m(k,\rho) &= -i\omega A_\rho^m(k,\rho) - \frac{\partial V^m(k,\rho)}{\partial\rho} \\ &= -i\omega(A_\rho^m(k,\rho) - \frac{A_\rho^m(k,\rho_0) I'_m(k\rho)}{I'_m(k\rho_0)}), \end{aligned} \tag{3.32}$$

$$\begin{aligned} E_\phi^m(k,\rho) &= -i\omega A_\phi^m(k,\rho) - \frac{1}{\rho}\frac{\partial V^m(k,\rho)}{\partial\phi} \\ &= -i\omega(A_\phi^m(k,\rho) - \frac{im}{k\rho}\frac{A_\rho^m(k,\rho_0) I_m(k\rho)}{I'_m(k\rho_0)}), \end{aligned} \tag{3.33}$$

$$\begin{aligned} E_z^m(k,\rho) &= -i\omega A_z^m(k,\rho) - \frac{\partial V^m(k,\rho)}{\partial z} \\ &= -i\omega(A_z^m(k,\rho) - i\frac{A_\rho^m(k,\rho_0) I_m(k\rho)}{I'_m(k\rho_0)}), \end{aligned} \tag{3.34}$$

and for $\rho > \rho_0$:

$$E_\rho^m(k,\rho) = -i\omega(A_\rho^m(k,\rho) - \frac{A_\rho^m(k,\rho_0)I_m(k\rho)K'_m(k\rho)}{I'_m(k\rho_0)K_m(k\rho_0)}), \tag{3.35}$$

$$E_\phi^m(k,\rho) = -i\omega(A_\phi^m(k,\rho) - \frac{im}{k\rho}\frac{A_\rho^m(k,\rho_0)I_m(k\rho_0)K_m(k\rho)}{I'_m(k\rho_0)K_m(k\rho_0)}), \tag{3.36}$$

$$E_z^m(k,\rho) = -i\omega(A_z^m(k,\rho) - i\frac{A_\rho^m(k,\rho_0)I_m(k\rho_0)K_m(k\rho)}{I'_m(k\rho_0)K_m(k\rho_0)}). \tag{3.37}$$

Vector potential equations

In the study by Bowtell et al. [1], the vector potential, $\vec{A}$ is found using the current passing through the coil. For cylindrical coil, with radius, the current is defined as:

$$\vec{J}^{coil}(\rho) = (\hat{\phi}J_\phi(\phi,z) + \hat{z}J_z(\phi,z))\delta(\rho - a), \tag{3.38}$$

where $\hat{\phi}$ and $\hat{z}$ are unit vectors in the directions of ϕ and z, respectively, $J_\phi(\phi,z)$, $J_z(\phi,z)$ are the surface current densities in ϕ and z directions and $\delta(\rho-a)$ is the delta function that describes the current at $\rho = a$, where a is the radius of the coil. Due to the characteristics of the coil, no current flows in the ρ-direction, so $J_\rho(\phi,z) = 0$.

Similar to the solution of Laplace's equation both $J_\phi(\phi,z)$ and $J_z(\phi,z)$ are in the form of:

$$J(\phi,z) = \frac{1}{2\pi}\sum_{m=-\infty}^{\infty} e^{im\phi}\int_{-\infty}^{\infty} e^{ikz}J^m(k)dk. \tag{3.39}$$

$J_\phi(\phi,z)$ and $J_z(\phi,z)$ can be written in terms of each other using the conservation of the charge relation, $\nabla\cdot\vec{J}^{coil} = -i\omega\rho_f$. As mentioned in Eq. (3.17) again by using the orthogonality, in the absence of charge accumulation (i.e., $\rho_f = 0$), the relation between the current components becomes:

$$\frac{m}{a}J_\phi^m(k) = -kJ_z^m(k). \tag{3.40}$$

To find the vector potential, the Eq.(3.12) is solved in phasor domain. The general vector potential-current relation is known as:

$$\vec{A}(\vec{r}) = \frac{\mu_0}{4\pi} \int \frac{\vec{J}^{coil}(\vec{r'})}{|\vec{r} - \vec{r'}|} d^3\vec{r'}, \tag{3.41}$$

and in Cartesian coordinates components of the vector potential are:

$$A_x(\vec{r}) = \frac{\mu_0}{4\pi} \int \frac{J_x^{coil}(\vec{r'})}{|\vec{r} - \vec{r'}|} d^3\vec{r'}, \tag{3.42}$$

$$A_y(\vec{r}) = \frac{\mu_0}{4\pi} \int \frac{J_y^{coil}(\vec{r'})}{|\vec{r} - \vec{r'}|} d^3\vec{r'}, \tag{3.43}$$

$$A_z(\vec{r}) = \frac{\mu_0}{4\pi} \int \frac{J_z^{coil}(\vec{r'})}{|\vec{r} - \vec{r'}|} d^3\vec{r'}. \tag{3.44}$$

In order to obtain vector potential components in cylindrical coordinates, first, according to the defined current, Eq.(3.38), the currents J_x and J_y are defined in cylindrical coordinates such as $J_x = -J'_\phi \sin\phi'$ and $J_y = J'_\phi \cos\phi'$ and then, vector potential components are written in cylindrical coordinates by using the following relations:

$$A_\rho = A_x \cos\phi + A_y \sin\phi, \tag{3.45}$$

$$A_\phi = -A_x \sin\phi + A_y \cos\phi. \tag{3.46}$$

As a result, the components of the vector potential become [33]:

$$A_\rho = \frac{\mu_0}{4\pi} \int \frac{J'_\phi(\vec{r'}) sin(\phi - \phi')}{|\vec{r} - \vec{r'}|} dv', \tag{3.47}$$

$$A_\phi = \frac{\mu_0}{4\pi} \int \frac{J'_\phi(\vec{r'}) cos(\phi - \phi')}{|\vec{r} - \vec{r'}|} dv', \tag{3.48}$$

$$A_z = \frac{\mu_0}{4\pi} \int \frac{J_z(\vec{r'})}{|\vec{r} - \vec{r'}|} dv'. \tag{3.49}$$

$\frac{1}{|\vec{r}-\vec{r'}|}$ can be defined according to Green's function expansion as:

$$\frac{1}{|\vec{r} - \vec{r'}|} = \frac{1}{\pi} \sum_{m=-\infty}^{\infty} e^{im(\phi-\phi')} \int_{-\infty}^{\infty} e^{ik(z-z')} dk I_m(k\rho <) K_m(k\rho >), \tag{3.50}$$

where $\rho < (\rho >)$ is the lesser (greater) of ρ and ρ'.

First, Eq.(3.50) is embedded to the Eq.(3.47), and this equation becomes:

$$A_\rho = \frac{\mu_0}{4\pi} \frac{1}{\pi} \sum_{m=-\infty}^{\infty} \int_{-\infty}^{\infty} \int_{-\infty}^{\infty} \int_{-\pi}^{\pi} \int_{0}^{\infty} e^{im\phi} e^{-im\phi'} e^{ikz} e^{-ikz'} I_m(k\rho <) K_m(k\rho >) J_{\phi'}(\phi', z')$$

$$\times \quad \delta(\rho'-a)(\frac{e^{i\phi}e^{-i\phi}-e^{-i\phi}e^{i\phi'}}{2i})\rho' d\rho' d\phi' dz' dk, \tag{3.51}$$

$$A_\rho = \frac{\mu_0 a}{i8\pi}\frac{1}{\pi}\sum_{m=-\infty}^{\infty}\int_{-\infty}^{\infty}\int_{-\infty}^{\infty}\int_{-\pi}^{\pi} e^{im\phi}e^{ikz}e^{-ikz'}I_m(k\rho<)K_m(k\rho>)J_{\phi'}(\phi',z')$$
$$\times \quad (e^{i\phi}e^{-i(m+1)\phi}-e^{-i\phi}e^{i(m-1)\phi'})d\phi' dz' dk. \tag{3.52}$$

In order to simplify Eq.(3.52), $J_\phi(\phi,z)$ and $J_z(\phi,z)$ are defined in the form of a Fourier Transform, such as:

$$J_z^m(k) = \frac{1}{2\pi}\int_{-\pi}^{\pi} d\phi e^{-im\phi}\int_{-\infty}^{\infty} dz e^{-ikz}J_z(\phi,z), \tag{3.53}$$

$$J_\phi^m(k) = \frac{1}{2\pi}\int_{-\pi}^{\pi} d\phi e^{-im\phi}\int_{-\infty}^{\infty} dz e^{-ikz}J_\phi(\phi,z). \tag{3.54}$$

By using Eq.(3.54) in the Eq.(3.51):

$$A_\rho = \frac{\mu_0 a}{i4\pi}\sum_{m=-\infty}^{\infty}\int_{-\infty}^{\infty} e^{im\phi}e^{ikz}(I_m(k\rho<)K_m(ka)J_\phi^{m+1}(k)e^{im\phi}$$
$$- \quad I_m(k\rho<)K_m(ka)J_\phi^{m-1}(k)e^{-im\phi})dk \tag{3.55}$$

and according to the general expression of A_ρ given in the form of Eq.(3.23), in this equation $A_\rho^m(k,\rho)$ is defined as:

$$A_\rho^m(k,\rho) = \frac{\mu_0 a}{i2}J_\phi(k)\{I_{m-1}(k\rho)K_{m-1}(ka) - I_{m+1}(k\rho)K_{m+1}(ka)\}. \tag{3.56}$$

By following the same procedure $A_\phi^m(k,\rho)$ and $A_z^m(k,\rho)$ components are:

$$A_\phi^m(k,\rho) = \frac{\mu_0 a}{2}J_\phi(k)\{I_{m-1}(k\rho)K_{m-1}(ka) + I_{m+1}(k\rho)K_{m+1}(ka)\}, \tag{3.57}$$

$$A_z^m(k,\rho) = \mu_0 a J_z(k)I_m(k\rho)K_m(ka). \tag{3.58}$$

By using the recurrence relations of the Bessel's Functions [34]:

$$I_n'(x) = I_{n-1}(x) - \frac{n}{x}I_n x, \tag{3.59}$$

$$K_{n+1}(x) = K_{n-1}(x) + \frac{2n}{x}K_n x, \tag{3.60}$$

$$K_n'(x) = -K_{n-1}(x) - \frac{n}{x}K_n x \tag{3.61}$$

in Eq.(3.56), (3.57) and (3.58), vector potential equations are:

$$A_\rho^m(k,\rho) = i\mu_0 a J_\phi^m(k)\{\frac{m}{k\rho}I_m(k\rho)K_m'(ka) + \frac{m}{ka}I_m'(k\rho)K_m(ka), \tag{3.62}$$

$$A_\phi^m(k,\rho) = -\mu_0 a J_\phi^m(k)\{I_m'(k\rho)K_m'(ka) + \frac{m^2}{k^2\rho a} I_m(k\rho)K_m(ka), \quad (3.63)$$

$$A_z^m(k,\rho) = \mu_0 a J_z(k) I_m(k\rho)K_m(ka). \quad (3.64)$$

There is no change on the vector potential inside and outside of the body.

To obtain the magnetic field expression, the Eq.(3.5) that gives the relation between the vector potential, and magnetic field is used:

$$\vec{B} = \nabla \times \vec{A}(\vec{r},t),$$

$$\vec{B} = \hat{\rho}(\frac{1}{\rho}\frac{\partial A_z}{\partial \phi} - \frac{\partial A_\rho}{\partial z}) + \hat{\phi}(\frac{\partial A_\rho}{\partial z} - \frac{\partial A_z}{\partial \rho}) + \hat{z}(\frac{1}{\rho}\frac{\partial \rho A_\phi}{\partial \rho} - \frac{1}{\rho}\frac{\partial A_\rho}{\partial \phi}). \quad (3.65)$$

Due to orthogonality, B^m components in the general magnetic field expression become:

$$B_\rho^m(k,\rho) = \frac{im}{\rho}A_z^m(k,\rho) - ikA_\phi^m(k,\rho), \quad (3.66)$$

$$B_\phi^m(k,\rho) = ikA_z^m(k,\rho) - \frac{\partial A_z^m(k,\rho)}{\partial \rho}, \quad (3.67)$$

$$B_\phi^m(k,\rho) = \frac{1}{\rho}\frac{\partial \rho A_\phi^m}{\partial \rho} - \frac{im}{\rho}A_\rho^m(k,\rho). \quad (3.68)$$

The equation (3.40), recurrence relation (3.59) and the equations for A_ρ^m (3.62), for A_ϕ^m (3.63) and for A_z^m (3.64) are used in the equations (3.66), (3.67) and (3.68). The resultant expressions are given below:

$$B_\rho^m(k,\rho) = i\mu_0 ka J_\phi^m(k) I_m'(k\rho)K_m'(ka), \quad (3.69)$$

$$\begin{aligned} B_\phi^m(k,\rho) &= ik\{i\mu_0 a J_\phi^m(k)\frac{\mu_0}{k\rho}I_m(k\rho)K_m'(ka) + i\frac{\mu_0 m}{k}J_\phi^m(k)I_m'(k\rho)K_m(ka)\} \\ &- \mu_0 ka J_z^m(k) I_m'(k\rho)K_m(ka) \\ &= -\frac{\mu_0 m a}{\rho}J_\phi^m(k)I_m(k\rho)K_m'(ka), \end{aligned} \quad (3.70)$$

$$\begin{aligned} B_z^m(k,\rho) &= \frac{m-1}{\rho}\mu_0 a J_\phi^m(k)K_m'(ka)\{I_m'(k\rho) + \frac{m}{k\rho}I_m k\rho - I_{m-1}(k\rho)\} \\ &- \mu_0 ka J_\phi^m(k) I_m(k\rho)K_m'(ka) \\ &= -\mu_0 ka J_\phi^m(k) I_m(k\rho)K_m'(ka). \end{aligned} \quad (3.71)$$

When the equations (3.62), (3.63) and (3.64) are used in (3.32), (3.33) and (3.34), the electric field components inside the body become as the following:

$$E_\rho^m(k,\rho) = \omega\mu_0 a\frac{m}{k}J_\phi^m(k)K_m'(ka)\{\frac{1}{\rho}I_m(k\rho) - \frac{I_m(k\rho_0)I_m'(k\rho)}{\rho_0 I_m'(k\rho_0)}\}, \quad (3.72)$$

$$E_{\phi}^{m}(k,\rho) = i\omega\mu_0 a J_{\phi}^{m}(k) K_m'(ka)\{I_m'(k\rho) - \frac{m^2}{k^2\rho\rho_0}\frac{I_m(k\rho)I_m(k\rho_0)}{I_m'(k\rho_0)}\}, \quad (3.73)$$

$$\begin{aligned} E_{z}^{m}(k,\rho) &= -i\omega\mu_0 a(J_{z}^{m}(k) I_m(k\rho) K_m(ka) \\ &+ J_{\phi}^{m}(k)\{\frac{m}{k\rho_0} I_m(k\rho_0) K_m'(ka) + \frac{m}{ka} I_m'(k\rho_0) K_m(ka)\}\frac{I_m(k\rho)}{I_m'(k\rho_0)}) \\ &= -i\frac{\omega\mu_0 am}{k\rho_0} J_{\phi}^{m}(k)\frac{I_m(k\rho)I_m(k\rho_0)K_m'(ka)}{I_m'(k\rho_0)}. \end{aligned} \quad (3.74)$$

After inserting the expressions of the fields into the Eq.(3.23) electric and magnetic field patterns inside the body are obtained in the study [1]. However, first, the transforms and integrals should be numerically evaluated for certain current distributions of any cylindrical coil. Without such a computational work, it is difficult to understand these field distributions.

3.2 Simplification of the Analytical Calculations of the Electric Field

To understand the field distribution inside and outside of the body more easily, magnetic and electric field expressions obtained by Bowtell [1] and described in the first section of this chapter, are simplified.

According to the defined current pattern, the magnetic and electric field patterns inside the gradient coil can be obtained. If the magnetic field distribution in the z-direction is known, the current distribution can be found and the electric field pattern inside and outside of the body can be observed. The relationship between the current density in ϕ-direction and the magnetic field in z-direction is:

$$J_{\phi}^{m} = -\frac{B_z^m}{\mu_0 ka I_m(k\rho) K_m'(ka)}. \quad (3.75)$$

To obtain simple expressions for the fields, target fields for x, y, and z-gradient coils are used as defined in the Chapter 2.

For x-gradient coil, the target field is taken as $B_z(\rho,\phi,z) = G_x x g(z) =$

$G_x\rho g(z)\cos\phi$ where G_x is the gradient field in phasor domain and $g(z)$ describes the z variation as mentioned in Chapter 2. To find J_ϕ^m, first B_z^m should be defined for the given target field [26]:

$$B_z^m = \frac{1}{2\pi}\int_{-\infty}^{\infty}\int_{-\pi}^{\pi} e^{-im\phi}\cos\phi e^{-ikz}G_x\rho g(z)d\phi dz \tag{3.76}$$

$$= \frac{1}{2\pi}\int_{-\infty}^{\infty}\int_{-\pi}^{\pi} e^{-im\phi}(\frac{e^{i\phi}+e^{-i\phi}}{2})e^{-ikz}G_x\rho g(z)d\phi dz \tag{3.77}$$

$$= G_x\rho\frac{\delta(m-1)+\delta(m+1)}{2}\int_{-\infty}^{\infty} g(z)e^{-ikz}dz. \tag{3.78}$$

For $g(k)=\int_{-\infty}^{\infty} g(z)e^{-ikz}dz$:

$$B_z^m = G_x\rho\frac{\delta(m-1)+\delta(m+1)}{2}g(k). \tag{3.79}$$

By inserting this B_z^m field into the Eq.(3.75) we can write the expression for J_ϕ^m as the following:

$$J_\phi^m = -\frac{G_x\rho[\delta(m-1)+\delta(m+1)]g(k)}{2\mu_0 kaI_m(k\rho)K'_m(ka)}. \tag{3.80}$$

By using Eq.(3.80) in the field equations in the form of $U_c^m(k,\rho)$, and embedding them to the equations in the form of (3.23), simplification is performed for all field components:

$$E_\rho(\rho,\phi,z) = -\omega G_x\rho\frac{1}{2\pi}\sum_{m=-\infty}^{\infty} e^{im\phi}\int_{-\infty}^{\infty} e^{ikz}\frac{m[\delta(m-1)+\delta(m+1)]g(k)}{2k^2}$$
$$\times \ (\frac{1}{\rho}-\frac{I_m(k\rho_0)I'_m(k\rho)}{\rho_0 I_m(k\rho)I'_m(k\rho_0)})dk, \tag{3.81}$$

$$E_\phi(\rho,\phi,z) = -i\omega G_x\rho\frac{1}{2\pi}\sum_{m=-\infty}^{\infty} e^{im\phi}\int_{-\infty}^{\infty} e^{ikz}\frac{[\delta(m-1)+\delta(m+1)]g(k)}{2k}$$
$$\times \ (\frac{I'_m(k\rho)}{I_m(k\rho)}-\frac{m^2 I_m(k\rho_0)}{k^2\rho\rho_0 I'_m(k\rho_0)})dk, \tag{3.82}$$

$$E_z(\rho,\phi,z) = -\omega G_x\rho\frac{1}{2\pi}\sum_{m=-\infty}^{\infty} e^{im\phi}\int_{-\infty}^{\infty} e^{ikz}\frac{m[\delta(m-1)+\delta(m+1)]I_m(k\rho_0)}{2k^2\rho_0 I'_m(k\rho_0)}$$
$$\times \ g(k)dk, \tag{3.83}$$

$$B_\rho(\rho,\phi,z) = -iG_x\rho\frac{1}{2\pi}\sum_{m=-\infty}^{\infty} e^{im\phi}\int_{-\infty}^{\infty} e^{ikz}\frac{[\delta(m-1)+\delta(m+1)]I'_m(k\rho)}{2I_m(k\rho)}$$
$$\times \ g(k)dk, \tag{3.84}$$

$$B_\phi(\rho,\phi,z) = G_x\frac{1}{2\pi}\sum_{m=-\infty}^{\infty} e^{im\phi}\int_{-\infty}^{\infty} e^{ikz}\frac{m[\delta(m-1)+\delta(m+1)]}{2k}$$
$$\times \ g(k)dk. \tag{3.85}$$

Due to $\delta(m)$ function, the summation indices can easily be defined as $m = \pm 1$ and the expression becomes summation free. Besides, for the derivative of the modified Bessel's functions, we can use the following recurrence relations [34]:

$$I_n'(x) = I_{n-1}(x) - \frac{n}{x} I_n(x), \tag{3.86}$$

$$K_n'(x) = -K_{n-1}(x) - \frac{n}{x} K_n(x), \tag{3.87}$$

$$I_n(x) = I_{-n}(x), \tag{3.88}$$

$$K_n(x) = K_{-n}(x). \tag{3.89}$$

With these relations, the electric and magnetic field expressions are written in the form of:

$$E_\rho(\rho,\phi,z) = -\omega G_x \rho \frac{e^{i\phi} - e^{-i\phi}}{2} \frac{1}{2\pi} \int_{-\infty}^{\infty} e^{ikz} \left(\frac{1}{\rho} - \frac{1}{\rho_0} \frac{I_1(k\rho_0)(I_0(k\rho) - \frac{1}{k\rho} I_1(k\rho))}{I_1(k\rho)(I_0(k\rho_0) - \frac{1}{k\rho_0} I_1(k\rho_0))}\right) \times \frac{g(k)}{k^2} dk, \tag{3.90}$$

$$E_\phi(\rho,\phi,z) = -i\omega G_x \rho \frac{e^{i\phi} + e^{-i\phi}}{2} \frac{1}{2\pi} \int_{-\infty}^{\infty} e^{ikz} \frac{g(k)}{k} \left(\frac{(I_0(k\rho) - \frac{1}{k\rho} I_1(k\rho))}{I_1(k\rho)} - \left(\frac{I_1(k\rho_0)}{k^2 \rho \rho_0 (I_0(k\rho_0) - \frac{1}{k\rho_0} I_1(k\rho_0))}\right)\right) dk, \tag{3.91}$$

$$E_z(\rho,\phi,z) = -\omega G_x \rho \frac{e^{i\phi} - e^{-i\phi}}{2} \frac{1}{2\pi} \int_{-\infty}^{\infty} e^{ikz} \frac{I_1(k\rho_0)}{k\rho_0 (I_0(k\rho_0) - \frac{1}{k\rho_0} I_1(k\rho_0))} \times \left(\frac{g(k)}{k}\right) dk, \tag{3.92}$$

$$B_\rho(\rho,\phi,z) = -iG_x \rho \frac{e^{i\phi} + e^{-i\phi}}{2} \frac{1}{2\pi} \int_{-\infty}^{\infty} e^{ikz} \frac{(I_0(k\rho) - \frac{1}{k\rho} I_1(k\rho))}{I_1(k\rho)} g(k) dk, \tag{3.93}$$

$$B_\phi(\rho,\phi,z) = G_x \frac{e^{i\phi} - e^{-i\phi}}{2} \frac{1}{2\pi} \int_{-\infty}^{\infty} e^{ikz} \frac{g(k)}{k} dk. \tag{3.94}$$

In these electromagnetic field equations, the argument of the Bessel's functions contains $k\rho$ that becomes small for low frequencies (e.g., $(k\rho) \leq 6 \times 10^{-5}$ for $\rho \leq$(radius of the coil$= 0.3m$) and frequency, $f \leq$ 10 kHz) or ka that is also limited with the radius of the coil. Thus, using the small argument approximation of the modified Bessel's functions, they can be expressed as [34]:

$$I_1(k\rho) = \frac{k\rho}{2}\left(1 + \frac{(k\rho)^2}{8}\right), \tag{3.95}$$

$$I_0(k\rho) = 1 + \frac{(k\rho)^2}{4}, \tag{3.96}$$

$$K_1(k\rho) = \frac{1}{2}(\frac{k\rho}{2})^{-1}, \tag{3.97}$$

$$K_0(k\rho) = -\ln(k\rho). \tag{3.98}$$

By using these approximated expressions in the Eq.(3.90):

$$\begin{aligned} E_\rho(\rho,\phi,z) &= -i\omega G_x \rho \sin\phi \frac{1}{2\pi}\int_{-\infty}^{\infty} e^{ikz}\frac{g(k)}{k^2}(\frac{1}{\rho} - \frac{1}{\rho_0}\frac{\frac{k\rho_0}{4}(1+\frac{(k\rho_0)^2}{8})(1+\frac{3(k\rho)^2}{8})}{\frac{k\rho}{4}(1+\frac{(k\rho)^2}{8})(1+\frac{3(k\rho_0)^2}{8})})dk \\ &= -i\omega G_x \sin\phi \frac{1}{2\pi}\int_{-\infty}^{\infty} e^{ikz}\frac{g(k)}{k^2}\frac{(\frac{(k\rho_0)^2}{4} - \frac{(k\rho)^2}{4})}{(1+\frac{(k\rho)^2}{8})(1+\frac{3(k\rho_0)^2}{8})}dk. \end{aligned} \tag{3.99}$$

Beside the small argument approximation of the Bessel's functions, with the assumption $(k\rho)^2 \ll 1$ for $\rho \leq \rho_0$, simplified expressions for E_ρ, E_ϕ, E_z, B_ρ and B_ϕ become:

$$E_\rho(\rho,\phi,z) = -i\omega G_x \sin\phi(\frac{{\rho_0}^2 - \rho^2}{4})\frac{1}{2\pi}\int_{-\infty}^{\infty} e^{ikz}g(k)dk, \tag{3.100}$$

$$\begin{aligned} E_\phi(\rho,\phi,z) &= -i\omega G_x \rho \cos\phi \frac{1}{2\pi}\int_{-\infty}^{\infty} e^{ikz}\frac{g(k)}{k}(\frac{(1+\frac{3(k\rho)^2}{8})}{k\rho(1+\frac{(k\rho)^2}{8})} - \frac{k\rho_0(1+\frac{(k\rho_0)^2}{8})}{k^2\rho\rho_0(1+\frac{3(k\rho_0)^2}{8})})dk \\ &= -i\omega G_x \cos\phi(\frac{{\rho_0}^2 + \rho^2}{4})\frac{1}{2\pi}\int_{-\infty}^{\infty} e^{ikz}g(k)dk, \end{aligned} \tag{3.101}$$

$$\begin{aligned} E_z(\rho,\phi,z) &= -\omega G_x \rho \sin\phi \frac{1}{2\pi}\int_{-\infty}^{\infty} e^{ikz}\frac{g(k)}{k}\frac{(1+\frac{(k\rho_0)^2}{8})}{(1+\frac{3(k\rho_0)^2}{8})}dk \\ &= -\omega G_x \rho \sin\phi \frac{1}{2\pi}\int_{-\infty}^{\infty} e^{ikz}\frac{g(k)}{k}dk, \end{aligned} \tag{3.102}$$

$$\begin{aligned} B_\rho(\rho,\phi,z) &= -iG_x \cos\phi \frac{1}{2\pi}\int_{-\infty}^{\infty} e^{ikz}g(k)\rho(\frac{1+\frac{3(k\rho)^2}{8}}{k\rho(1+\frac{(k\rho)^2}{8})})dk \\ &= -iG_x \cos\phi \frac{1}{2\pi}\int_{-\infty}^{\infty} e^{ikz}\frac{g(k)}{k}dk, \end{aligned} \tag{3.103}$$

$$B_\phi(\rho,\phi,z) = iG_x \sin\phi \frac{1}{2\pi}\int_{-\infty}^{\infty} e^{ikz}\frac{g(k)}{k}dk. \tag{3.104}$$

As mentioned in Chapter 2, $g(z)$ is taken as $g(z) = 1$. If $g(z)$ is expressed as the given form in Chapter 2 (i.e., $g(z) = [1 + (\frac{z}{d})^6]^{-1}$), the inverse Fourier of $g(k)$ is not convergent. In order to get rid of this, during the design, another parameter is used in expressions [26], which is out of our scope when $g(z) = 1$. With this, the simplified electric and magnetic field expressions inside the body, $\rho < \rho_0$ become as following [35]:

$$E_\rho(\rho,\phi,z) = -i\omega G_x \sin\phi(\frac{{\rho_0}^2 - \rho^2}{4}), \tag{3.105}$$

$$E_\phi(\rho,\phi,z) = -i\omega G_x \cos\phi(\frac{{\rho_0}^2+\rho^2}{4}), \quad (3.106)$$

$$E_z(\rho,\phi,z) = -i\omega G_x \rho z \sin\phi, \quad (3.107)$$

$$B_\rho(\rho,\phi,z) = G_x z\cos\phi, \quad (3.108)$$

$$B_\phi(\rho,\phi,z) = -G_x z\sin\phi. \quad (3.109)$$

Outside the body ($\rho > \rho_0$), there is no change in the magnetic field expression. To find the electric field expressions one more assumption is used [34]:

$$\lim_{k\to 0} (k\rho)^n \ln(k\rho) \to 0 \ for\ n\ real\ constant\ and\ n > 0. \quad (3.110)$$

With this assumption the electric field expressions are;

$$E_\rho(\rho,\phi,z) = i\omega G_x \sin\phi(\frac{{\rho_0}^4+\rho^4}{4\rho^2}), \quad (3.111)$$

$$E_\phi(\rho,\phi,z) = -i\omega G_x \cos\phi(\frac{{\rho_0}^4+\rho^4}{4\rho^2}), \quad (3.112)$$

$$E_z(\rho,\phi,z) = -i\omega G_x \rho z \sin\phi. \quad (3.113)$$

For y and z-gradient coils, target fields are defined as $B_z(\rho,\phi,z) = G_y y g(z) = G_x \rho g(z)\sin\phi$ and $B_z(\rho,\phi,z) = G_z z g(z)$, respectively. Details of the simplification of the equations for these coils are given in Appendices A and B. Unlike x and y-coils, the current passing through the z-coil is defined as $J^{coil}(\rho) = \hat{\phi} J_\phi(\phi,z)\delta(\rho-a)$, so for this coil, the vector potential in z-direction, A_z is zero which can be understood from the Eq.(3.64). For y-gradient coil, the electric and magnetic field expressions inside the body are [35]:

$$E_\rho(\rho,\phi,z) = i\omega G_y \cos\phi(\frac{{\rho_0}^2-\rho^2}{4}), \quad (3.114)$$

$$E_\phi(\rho,\phi,z) = -i\omega G_y \sin\phi(\frac{{\rho_0}^2+\rho^2}{4}), \quad (3.115)$$

$$E_z(\rho,\phi,z) = i\omega G_y \rho z\cos\phi, \quad (3.116)$$

$$B_\rho(\rho,\phi,z) = G_y z\sin\phi, \quad (3.117)$$

$$B_\phi(\rho,\phi,z) = G_y z\cos\phi, \quad (3.118)$$

outside the body, the electric field expressions are:

$$E_\rho(\rho,\phi,z) = -i\omega G_y \cos\phi(\frac{{\rho_0}^4+\rho^4}{4\rho^2}), \quad (3.119)$$

$$E_\phi(\rho,\phi,z) = -i\omega G_y \sin\phi(\frac{{\rho_0}^4+\rho^4}{4\rho^2}), \quad (3.120)$$

$$E_z(\rho,\phi,z) = i\omega G_y \rho z \cos\phi. \quad (3.121)$$

And for z-gradient coil the electric and magnetic field expressions inside the body become [35]:

$$E_\rho(\rho,\phi,z) = 0, \quad (3.122)$$

$$E_\phi(\rho,\phi,z) = -i\omega G_z \frac{\rho}{2} z, \quad (3.123)$$

$$E_z(\rho,\phi,z) = 0, \quad (3.124)$$

$$B_\rho(\rho,\phi,z) = -G_z \frac{\rho}{2}, \quad (3.125)$$

$$B_\phi(\rho,\phi,z) = 0, \quad (3.126)$$

outside the body, the electric field expressions become:

$$E_\rho(\rho,\phi,z) = 0, \quad (3.127)$$

$$E_\phi(\rho,\phi,z) = -i\omega G_z \frac{\rho}{2} z, \quad (3.128)$$

$$E_z(\rho,\phi,z) = 0. \quad (3.129)$$

3.2.1 Field Patterns

To understand the accuracy of the resultant simplified expressions, the electric and magnetic field patterns are observed and these are compared with the resultant patterns of the previous study [1]. These patterns are obtained for a x-gradient coil with diameter 0.654 m, the gradient 20 mTm^{-1}, and the gradient switching rate 100 $Tm^{-1}s^{-1}$, and it is assumed that radius of the body model is 0.195 m. Figures 3.1 and 3.2 show these electric and magnetic field distributions. Each pattern is obtained inside the body model ($\rho < \rho_0$ where $\rho_0 = 0.195$ m). Along the z direction, only $z = \pm 0.39$ m region is shown, since the maximum magnetic field observed in study [1] is at $z = 0.39$ m and $\rho = \rho_0$, and after that point, for a real gradient coil, the field starts to decrease, but in our case due

to the linear field assumption, it continues to increase, so in order to compare the patterns obtained in this thesis and previous study [1] easily, only region $z = \pm 0.39\ m$ is used. This comparison is given in discussion section.

Because of the conductivity difference at the boundary, charge can be occurred, and due to the charge density, there is a discontinuity in the partial derivative of the scalar potential. This discontinuity can be observed at the ρ component of the electric field and also at the magnitude of the total electric field. Figure 3.3 shows the discontinuity at the electric field component. For three different angle values, along the ρ direction, the change in each field component, E_ρ, E_ϕ, E_z, pattern is observed. In E_ρ pattern, at $\rho = 0.195\ m$ discontinuity can easily be seen. In E_ϕ pattern, there is no discontinuity at the boundary, but the characteristics of the field is different inside and outside the body. In E_z pattern, there is no change, and the characteristics of the field is same both inside and outside the body.

3.2.2 Discussion

To obtain field expressions, it is assumed that there is no charge in the bulk of the body which means the divergence of the electric field should be zero. In order to check the accuracy of the simplified field equations, it is verified.

As expected, the resultant simplified magnetic field expressions are the same as the expressions given in the study [27] and also in Chapter 2, for perfectly uniform gradient fields. Moreover, in Chapter 2, the equivalent of $\frac{\partial B_y}{\partial x}$ and $\frac{\partial B_x}{\partial y}$ has been taken as zero and this is confirmed with the resultant expressions found in this chapter.

To observe the correct field patterns, the path of the current should be defined accurately. Probably, due to the difference of the current paths of the coil in

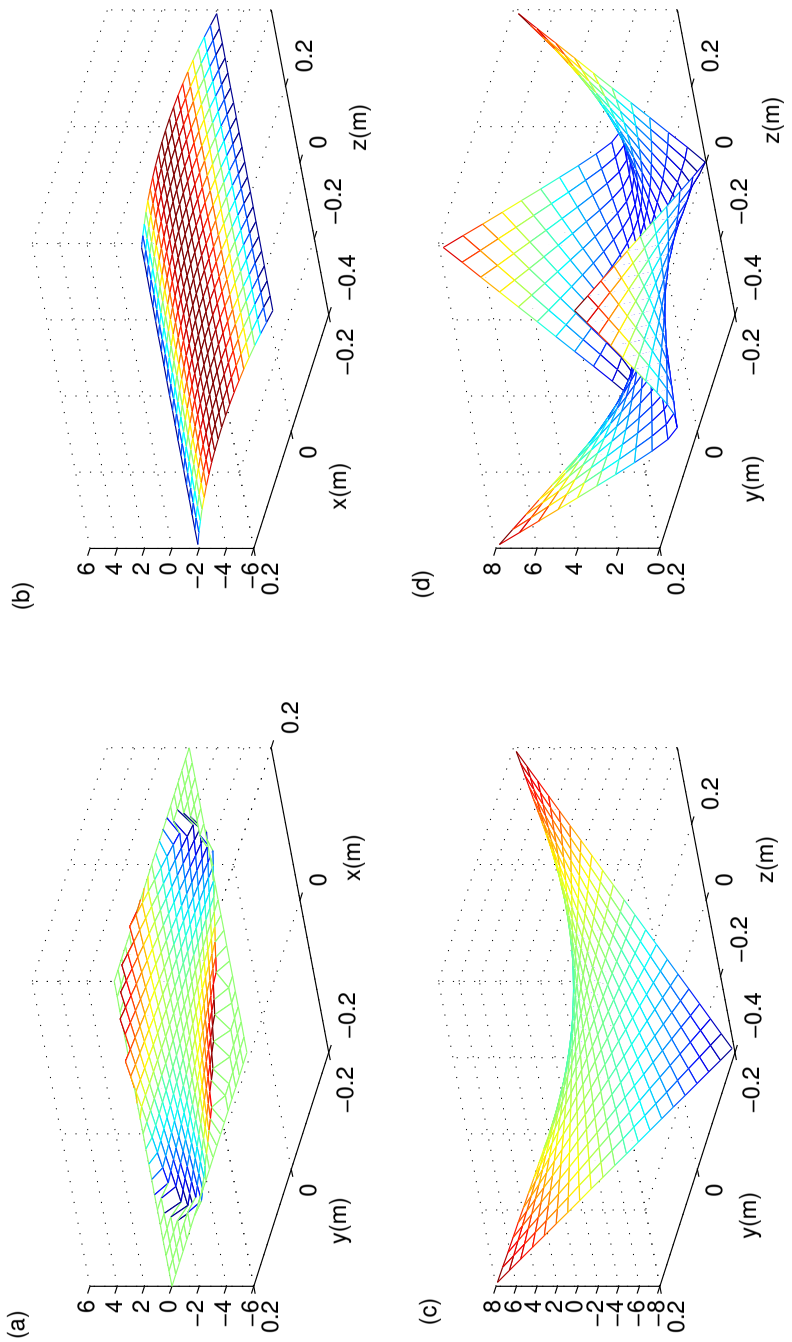

Figure 3.1: E-field distribution formed by the equation of our study for x-gradient coil. a: $E_x(y, x)$ for $z = 0$. b: $E_y(x, z)$ for $y = 0$. c: $E_z(y, z)$ for $x = 0$. d: $|E(y, z)|$ for $x = 0$.

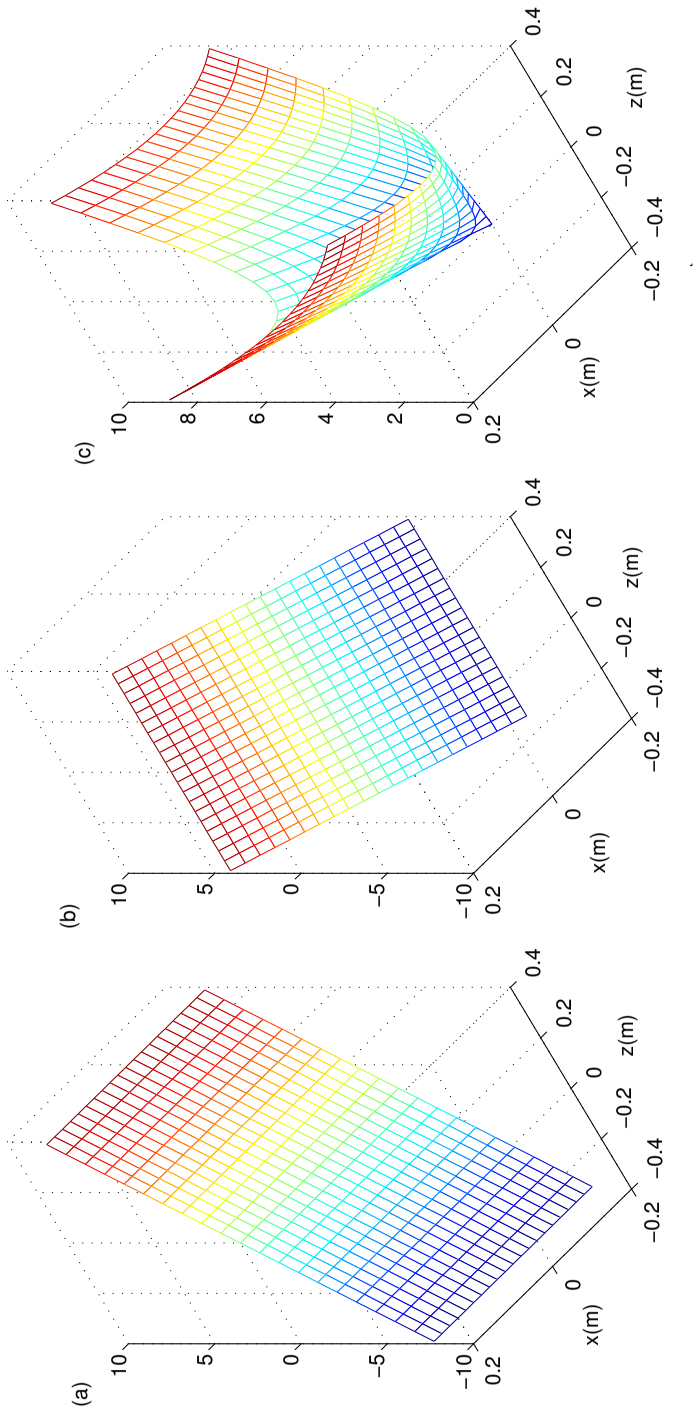

Figure 3.2: B-field distribution for x-gradient coil in our study. a: $B_x(x, z)$ for $y = 0$. b: $B_z(x, z)$ for $y = 0$. c: $|B(x, z)|$ for $y = 0$.

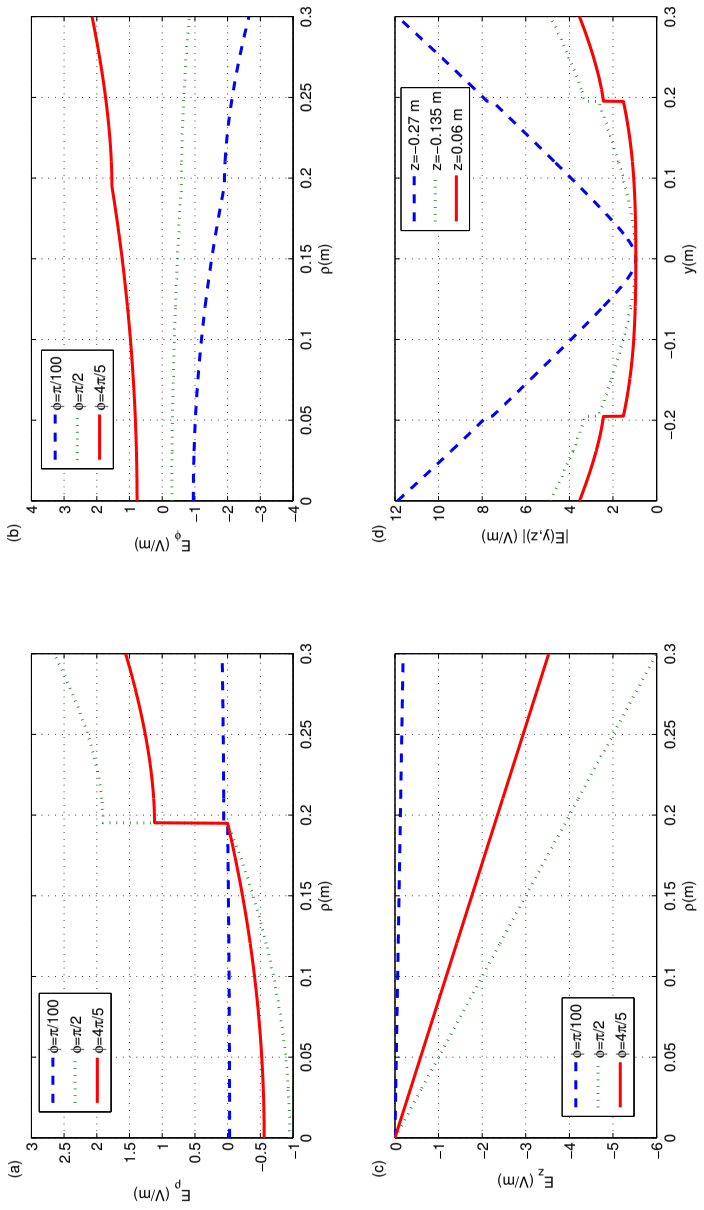

Figure 3.3: Discontinuity in E-field distribution for x-coil. a: Change in $E_\rho(\rho, \phi)$ according to $\rho(m)$ for x- coil, b: Change in $E_\phi(\rho, \phi)$ according to $\rho(m)$, c: Change in $E_z(\rho, \phi)$ according to $\rho(m)$, d: Change in $|E(y, z)|$ according to $y(m)$.

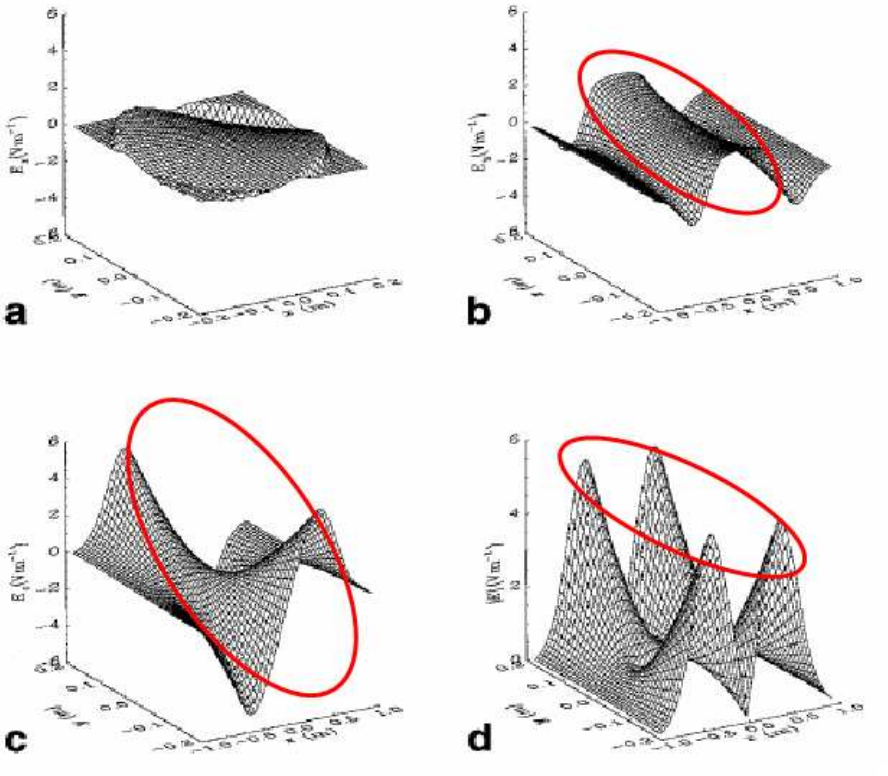

Figure 3.4: E-field distribution found by Bowley and Bowtell [1] for$x$-gradient coil. a: $E_x(y,x)$ for $z = 0$. b: $E_y(x,z)$ for $y = 0$. c: $E_z(y,z)$ for $x = 0$. d: $|E(y,z)|$ for $x = 0$

study [1], there are inconsistencies in E_x, E_y, and B_z field graphs obtained in this thesis. Figures 3.4 and 3.5 show the result of the study [1]. The comparison of the graphs obtained in two studies can be made in a certain region indicated in the figures. Since, the simplification of the equations are performed for a coil with a perfectly uniform gradient field, the characteristics of the graphs in both studies are the same in the volume of interest where the change at the linearity of the field is up to 5%.

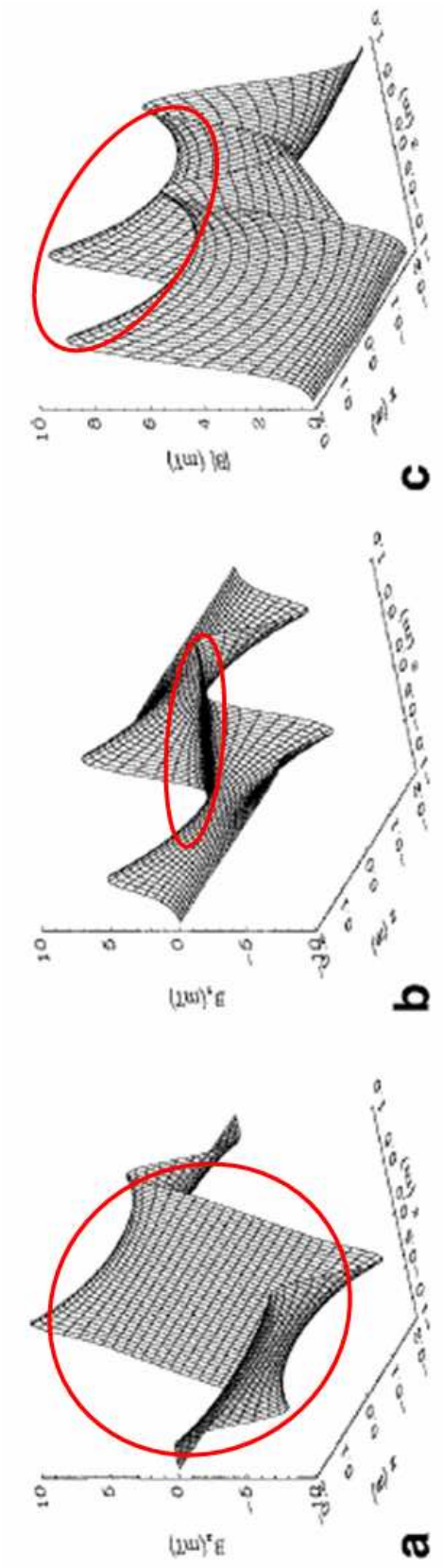

Figure 3.5: B-field distribution found by Bowley and Bowtell [1] for x-gradient coil. a: $B_x(x,z)$ for $y=0$. b: $B_z(x,z)$ for $y=0$. c: $|B(x,z)|$ for $y=0$.

Chapter 4

THE SAFETY CONCERN OF THE GRADIENT FIELD

Peripheral nerve stimulation (PNS) is one of the bioeffects of the time varying gradient field. If a certain magnitude electric field is applied during a sufficient duration, peripheral nervous system can be stimulated. During experimental studies volunteers report spatially localized sensations of pressure, or muscle twitching [13].

The nerve stimulation near an implant during magnetic resonance imaging has also been examined [2]. This is an important study to understand whether MR imaging techniques can be used on patients with an implant or not.

In order to understand the excitability of the nerve, first the strength-duration curve and the behavior of the nerve have been investigated. In the first section of this chapter the laws of nerve stimulation is introduced. Under the light of this knowledge, the other sections describe the worst position and length of an

implant that causes stimulation and determine the maximum length of the lead of a pacemaker.

4.1 Nerve Stimulation without an implant

Resting typical polarized cells are charged positively on the outside and negatively on the inside according to the distribution of K^+ ion. Electrical stimulus will bring the resting membrane potential to the threshold potential by changing the distribution of the Na^+ and K^+ ions [36]. In the region of a locally constant electric field, excitation is initiated where a nerve is ended, or undergoes a rapid bend, or at the point where the excitation is directly exposed. These modes are shown in Figure 4.1 [2]. The threshold of the excitation depends on the position of the nerve and the spatial distribution of the electric field. In study [2] different electric field threshold values for sufficient durations are given for 20 μm nerve fibers with different bending points and angles. The electric field is oriented parallel to the fiber. These electric field thresholds are presented in Table 4.1. The first column indicates the bend angle. The second column lists the nerve node at which the bend occurs. $E_{threshold}$ is the rheobase excitation threshold and $\tau_c(\mu s)$ is the strength duration time constant.

Table 4.1: Excitation requirements for a nerve with different modes of stimulation [2]

Bend angle(deg)	**number of the bend node**	$\mathbf{E_{threshold}}$ **(V/m)**	$\tau_\mathbf{c}(\mu\mathbf{s})$
0	1	6.21	128.2
90	2	8.55	126.0
90	8	9.96	112.9
180	2	6.56	101.4
180	6	5.10	110.3

In order to compare the electric field values with the results of the former studies and standards and also to understand the stimulation risk, the real gradient coil

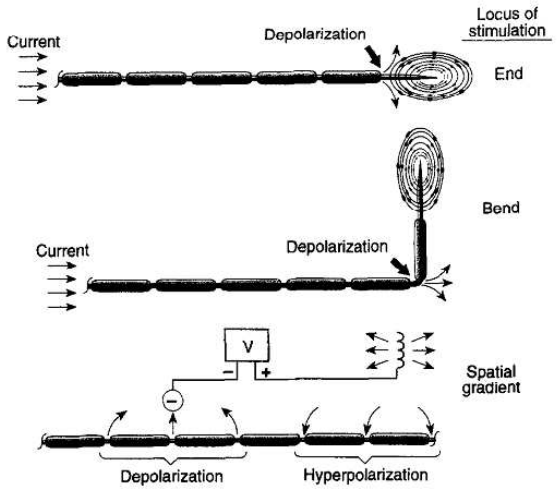

Figure 4.1: The neural stimulation modes [2]

parameters are used as given in Table 4.2. We check whether these parameters fall within the limits related to prevention of cardiac stimulation.

In order to understand the worst position for the maximum electric field, surface plots are observed for different radii. The maximum electric field magnitude is observed at the surface of the body model (i.e., $\rho = \rho_0$) and it is in the z-direction. For z-gradient coil, the electric field z and ρ components are zero and for other coils, distribution patterns are given in Figures 4.2 and 4.3.

Thus, at the surface of the body model, the expression of the total electromagnetic field produced by each gradient coil in the cylindrical coordinates is as the following:

$$\begin{aligned}
\vec{E}(\rho=\rho_0,\phi,z) &= G'_x(t)\{-0.5\rho_0^2\cos\phi\hat{\phi} - \rho_0 z\sin\phi\hat{z}\} + G'_y(t)\{-0.5\rho_0^2\sin\phi\hat{\phi} + \rho_0 z\cos\phi\hat{z}\} \\
&+ G'_z(t)\{-0.5\rho_0 z\hat{\phi}\}, \qquad (4.1) \\
\vec{B}(\rho=\rho_0,\phi,z) &= G_x(t)\{z\cos\phi\hat{\rho} - z\sin\phi\hat{\phi} + \rho_0\cos\phi\hat{z}\} \\
&+ G_y(t)\{z\sin\phi\hat{\rho} + z\cos\phi\hat{\phi} + \rho_0\sin\phi\hat{z}\} \\
&+ G_z(t)\{-0.5\rho_0\hat{\rho} + z\hat{z}\}. \qquad (4.2)
\end{aligned}$$

To understand the worst case for the electric field that causes the stimulation, Reilly [37] assumed that maximum z gradient magnetic field is in the z-direction

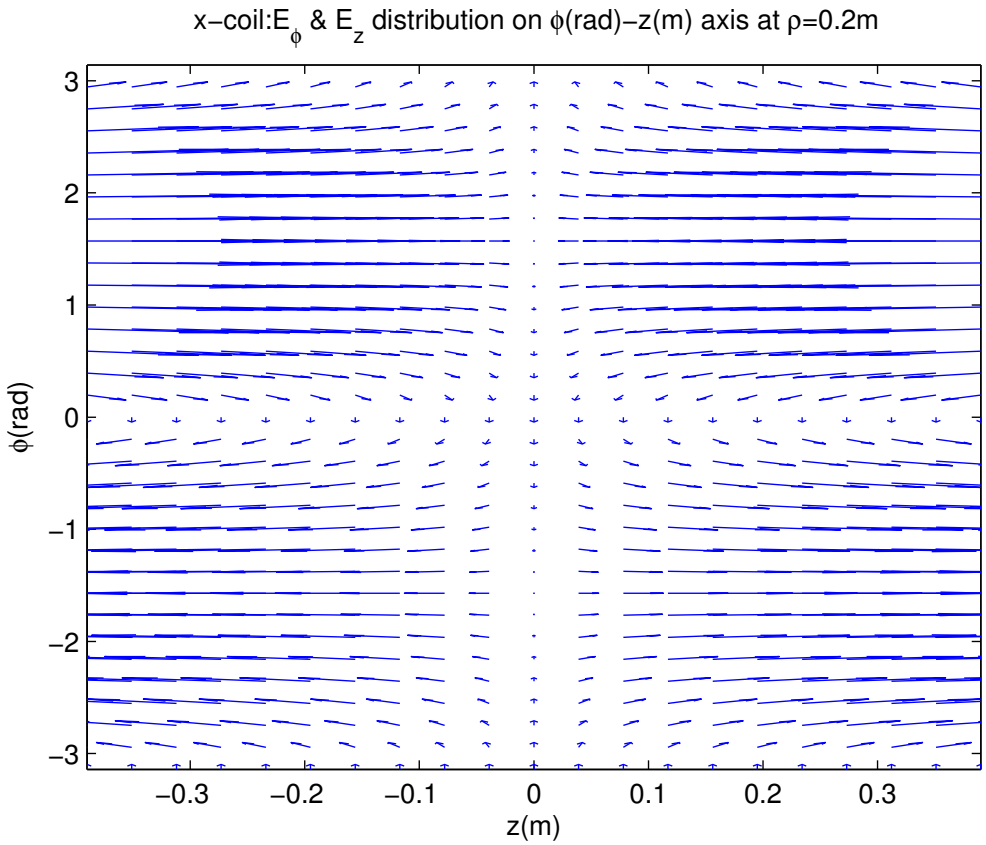

Figure 4.2: E_ϕ and E_z components distribution on the surface with $\rho = 0.2$ for x-gradient coil.

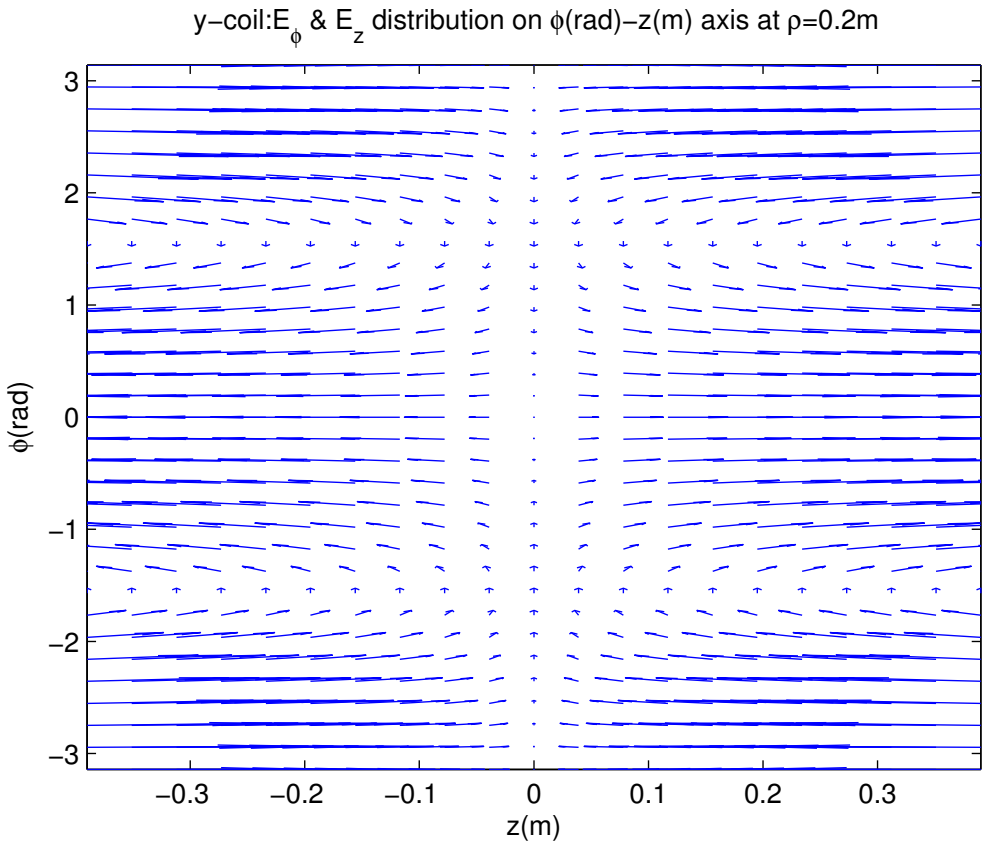

Figure 4.3: E_ϕ and E_z components distribution on the surface with $\rho = 0.2$ for y-gradient coil.

and uniform over a circular cross section of radius, ρ_0. For uniform magnetic field, relation between the magnetic and electric field are given as:

$$\vec{E} \cdot (2\pi\rho_0)\hat{\phi} = -(\pi\rho_0^2)\hat{z} \cdot \frac{\partial \vec{B}}{\partial t}, \tag{4.3}$$

$$|B_z'(t)| = 2|E_\phi(\rho)|/\rho_0, \tag{4.4}$$

where $B_z'(t)$ is the first order time derivative of the magnetic field in z-direction. With the simplified expressions for the maximum magnetic field same relation can be observed [35], however, the magnetic field has also a component in the ϕ-direction. For x and y-coils as mentioned before the electric field has a component in the z-direction and it is the dominant one to cause the stimulation.

When only x-gradient coil is effective, maximum electric field is observed at $\phi = \pi/2$ and $z = DSV/2$, where DSV is the diameter spherical volume with field homogeneity. When all coils are driven simultaneously with identical waveforms at the maximum slew rate ($\frac{\partial G}{\partial t}$), maximum electric field is observed at $\phi = \pi/4$ and $z = DSV/2$. These maximum electric field magnitudes in z-direction for a body model with a radius, $\rho_0 = 0.2\ m$ are given in Table 4.2.

Table 4.2: Maximum Electric Field Magnitudes in z-direction inside the human body model with radius, $\rho_0 = 0.2m$ according to the gradient coil parameters

Gradient Coil	$Magnetom Symphony 1.5T$	$Magnetom Avanto 1.5T$	$Signa CV/i$
DSV	$0.5m$	$0.5m$	$0.4m$
$\mathbf{G_x}$, $\mathbf{G_y}$, $\mathbf{G_z}$	$30mT/m$	$45mT/m$	$40mT/m$
$\frac{\partial \mathbf{G_x}}{\partial \mathbf{t}}$, $\frac{\partial \mathbf{G_y}}{\partial \mathbf{t}}$, $\frac{\partial \mathbf{G_z}}{\partial \mathbf{t}}$	$125T/m/sec$	$200T/m/sec$	$150T/m/sec$
Min. Rise Time	$240\mu s$	$225\mu s$	$267\mu s$
$\mathbf{E_z max\ x-coil}$	$6.25V/m$	$10V/m$	$6V/m$
$\mathbf{E_z max\ all\ coils}$	$8.84V/m$	$14.14V/m$	$8.48V/m$

Depending on the threshold values given in Table 4.1, it can be said that any nerve with a diameter of 20 μm and located parallel to the E_z field can be stimulated with the maximum electric field values obtained for the maximum slew rates supplied by different coils given in Table 4.2. When the diameter of

a fiber decreases, the threshold level will increase and the risk of the stimulation will decrease. For example the threshold for a fiber with a diameter of 10 μm is 12.3 V/m and for a fiber with a diameter of 5 μm it becomes 24.6 V/m [2]. These examples show that with any of the coils given in Table 4.2, 5 μm nerve may not be stimulated.

In the standards [38], to protect against peripheral nerve stimulation, the strength duration curve is defined as the relation between the rate of change of the magnetic field during gradient switching dB/dt (T/s), and the effective stimulus duration $t_{s,eff}(ms)$ or as the relation between the electric field E (V/m), and the effective stimulus duration $t_{s,eff}(ms)$ such that:

$$\frac{dB}{dt} = 20\{1 + \frac{0.36}{t_{s,eff}}\}, \tag{4.5}$$

$$E = 2.2\{1 + \frac{0.36}{t_{s,eff}}\}, \tag{4.6}$$

where "20" is the rheobase dB/dt (T/s) value, "2.2" is the rheobase E (V/m) value and "0.36" is the chronaxia time $\tau_c(\mu s)$. The values in these expressions are suited with the theoretical values of the threshold given in [39]. As mentioned before, Reilly has assumed a uniform z gradient magnetic field. According to our study, when dB/dt (T/s) value is converted to dG/dt (T/s) using the maximum field location($\rho = 0.2$ m and $z = DSV/2$), the electric field threshold becomes 1.89 V/m which is not much different than the value in eq.(4.6), used in standards and obtained by Reilly [39]. Stimulation risk for each coil given in Table 4.2 can be investigated with this strength-duration relation. For, Siemens Magnetom Symphony 1.5T, $t_{s,eff}$ is taken as 0.24 s, so maximum $\frac{dB}{dt} = 50$ T/s and then, maximum rate of change of the gradient at $\rho = 0.2$ m and $z = 0.25$ m should be 156 T/m, which is larger than the given value, and for the other coils, for Siemens Magnetom Avanto 1.5T, it is 162.4 T/m and for GE Signa CV/i, it is 166 T/m, these values are also comparable with the real parameters. But as found before, the stimulation risk with Siemens Magnetom Avanto 1.5T is higher than the other coils because of the high slew rate 200 T/m, and maximum electric

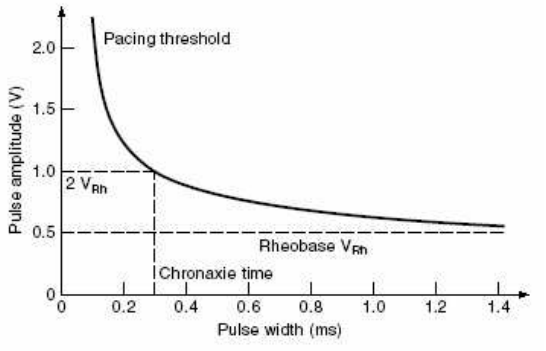

Figure 4.4: Pulse width-amplitude relation necessary for tissue stimulation. This graph is taken from [3].

field values also give the similar results with that conclusion. However, scanners are driven at the safety limits, defined by the standards [38].

Minimum threshold value for both cardiac and nerve tissue is the same. However, the excitation time constant of cardiac tissue is relatively longer [39].

In [3], strength-duration curve for the tissue is obtained. To obtain this curve, the tissue is stimulated with an impulse obtained from the output amplifier of the pacemaker. The amplitude is adjustable from 0.1 V to 9.6 V and also the pulse width is between 0.1 ms and 2 ms. The resultant graph is given in Figure 4.4. According to this result rheobase voltage is determined as 0.5 V.

4.2 The worst position and the minimum length of the implants causing stimulation

If there is an implant near a nerve, it may causes the stimulation during MRI. Reilly have worked on the relation between the position of the implant and the nerve and observed that the most sensitive case is when the nerve is terminated

near the wire tip and oriented parallel to the wire [2]. When the distance between the wire and the nerve increases, threshold of the field also increases [2].

To determine the minimum length of the implant lead that causes the stimulation, cardiac pacing threshold voltage is used. It is taken as 0.5 V according to [3]. For this value, the lengths of the implant leads starting from the point that the maximum electric fields obtained for the different coil parameters given in Table 4.2 are determined approximately by using the relationship $V = \int \vec{E} \cdot \vec{dl}$, and this integral is calculated along the wire. The position of the nerve is assumed to be parallel to the implant and also to E_z field. The minimum implant lead length values for different coil parameters are given in Table 4.3. Using the rheobase value and chronaxia time given in standards [38] such as $E_{threshold} = 2.2\ V/m$ and $\tau_c = 0.36\ \mu s$ the lead length value is obtained as 11 cm.

Table 4.3: Minimum Implant Lead Length to stimulate the nerve at the maximum electric field.

Gradient Coil	$MagnetomSymphony1.5T$	$MagnetomAvanto1.5T$	$SignaCV/i$
length(cm) – x – coil	8	5.5	6.2
length(cm) – all coils	5.67	3.9	4.3

4.3 The maximum length of the lead of a pacemaker for MR safety

The location of the pacemaker, based on the evaluation of the dimensions of typical lead position given in [40], can be used to understand the stimulation risk due to the induced voltage on the lead. When the umbilicus is taken as the center of the coil, the heart location is in approximately 20 cm distance from the center. ICD (implantable cardioverter defibrillator) is located at 10 cm above

the heart. Human heart can be modeled as a sphere with a radius 3 cm and the distance between heart center and the torso center is taken as 5 cm. Leads will be located at the right atrium, right ventricle and left ventricle. In order to understand the simple case, it is assumed that lead directly goes to the heart, by following the line, parallel with the distance 3 cm to the line passing on the torso center. Generally the length of a pacemaker lead is longer than 40 cm. For a lead length of 50 cm, the length from the ICD to the heart is taken as 15 cm, and there are two loops around the ICD. At this location along the strength part of the lead the magnitude of the maximum electric field in z-direction is for Siemens Magnetom Symphony 1.5T, 1.125 V/m, for Siemens Magnetom Avanto 1.5T, 1.8 V/m, for GE Signa CV/i, 1.35 V/m. These electric field values are obtained when only x-coil is effective. For the loops, ρ components of the electric fields are used. With these values, voltages induced on the lead become 0.36 V, 0.547 V and 0.41 V, respectively. These values are comparable with the pacing threshold voltage. When each gradient field is effective simultaneously with identical waveforms, the maximum electric field values are for Magnetom Symphony 1.5T, 1.6 V/m, for Magnetom Avanto 1.5T, 2.56 V/m, for Signa CV/i, 1.9 V/m and voltage values become 0.52 V, 0.77 V and 0.58 V, respectively. These values show that there is stimulation risk for the patient with pacemakers in MRI.

These voltage values are approximate results. To understand the risk of the electric field to the pacemaker more clearly, the current passing through the lead should also be investigated. To calculate this current, first, the relation between the tissue and the lead tip should be investigated as a circuit model which will be investigated as a future study.

Chapter 5

CONCLUSION AND FUTURE WORK

As a summary, in this thesis, simple expressions for the electric field inside and outside the cylindrical homogenous body model for a perfectly uniform gradient field are derived. These simple expressions are used to understand the nerve-stimulation thresholds.

First, in order to understand the relationship between the current passing through the coil and the gradient field, design procedures are investigated. Simplification is performed by using the target field method approach. Under the quasi-static assumptions and appropriate boundary condition, the analytical expressions can easily be obtained. These expressions are directly related with the current. By using the defined target field for perfectly uniform magnetic field, the current is obtained. With this current, the field expressions are simplified and we have obtained general field expressions formed inside and outside of a cylindrical homogenous body model. With this simplified expressions, for different coil properties, maximum electric field values are achieved. These values are used to understand the nerve and cardiac stimulation risk. According to these

values nerve stimulation can be observed for 20 μm and 10 μm nerves, if the field is parallel to the nerve. By using the cardiac pacing voltage, the worst implant lead length is determined such that it should be bigger than 4 cm to cause the stimulation.

Our future work will consist of implant-tissue relationship for stimulation. Because of the impedance between the implant lead and the tissue, current will flow through the lead. The interaction of an implant and the gradient field should be investigated clearly to understand the safe operation conditions exactly. To check the analytical results and to obtain the impedance model more easily, the gradient field will be modeled by using plane waves. As a result, simulation region can be formed easily rather than the field generated by the gradient coil.

APPENDIX A

Simplification of the Electric Field Expressions for y-gradient coil

For y-gradient coil, target field is $B_z(\rho,\phi,z) = G_y y g(z) = G_x \rho g(z)\sin\phi$ and the relation between J_ϕ^m and B_z^m is $J_\phi^m(k) = i\frac{G_y\rho[\delta(m-1)-\delta(m+1)]}{2\mu_0 k a I_m(k\rho)K'_m(ka)}g(k)$. According to that, fields become:

$$\begin{aligned}
E_\rho(\rho,\phi,z) &= i\omega G_y\rho\frac{1}{2\pi}\sum_{m=-\infty}^{\infty}e^{im\phi}\int_{-\infty}^{\infty}e^{ikz}\frac{m[\delta(m-1)-\delta(m+1)]g(k)}{2k^2} \\
&\times \ (\frac{1}{\rho}-\frac{I_m(k\rho_0)I'_m(k\rho)}{\rho_0 I_m(k\rho)I'_m(k\rho_0)})dk, \qquad \text{(A.1)} \\
E_\phi(\rho,\phi,z) &= -\omega G_y\rho\frac{1}{2\pi}\sum_{m=-\infty}^{\infty}e^{im\phi}\int_{-\infty}^{\infty}e^{ikz}\frac{[\delta(m-1)-\delta(m+1)]g(k)}{2k} \\
&\times \ (\frac{I'_m(k\rho)}{I_m(k\rho)}-\frac{m^2 I_m(k\rho_0)}{k^2\rho\rho_0 I'_m(k\rho_0)})dk, \qquad \text{(A.2)} \\
E_z(\rho,\phi,z) &= \omega G_y\rho\frac{1}{2\pi}\sum_{m=-\infty}^{\infty}e^{im\phi}\int_{-\infty}^{\infty}e^{ikz}\frac{[\delta(m-1)-\delta(m+1)]I_m(k\rho_0)}{2\rho_0 I'_m(k\rho_0)} \\
&\times \ \frac{g(k)}{k^2}dk, \qquad \text{(A.3)} \\
B_\rho(\rho,\phi,z) &= -G_y\rho\frac{1}{2\pi}\sum_{m=-\infty}^{\infty}e^{im\phi}\int_{-\infty}^{\infty}e^{ikz}\frac{[\delta(m-1)-\delta(m+1)]I'_m(k\rho)}{2I_m(k\rho)}
\end{aligned}$$

$$\times \quad g(k)dk, \tag{A.4}$$

$$B_\phi(\rho,\phi,z) = -iG_y\frac{1}{2\pi}\sum_{m=-\infty}^{\infty} e^{im\phi}\int_{-\infty}^{\infty} e^{ikz}\frac{m[\delta(m-1)-\delta(m+1)]}{2}$$

$$\times \quad \frac{g(k)}{k}dk. \tag{A.5}$$

Due to $\delta(m)$ function, the summation indices are defined as $m = \pm 1$ and the expressions become summation free; besides, by using recurrence relations for Bessel's functions given in Chapter 3, the expressions are:

$$E_\rho(\rho,\phi,z) = i\omega G_y\rho\cos\phi\frac{1}{2\pi}\int_{-\infty}^{\infty} e^{ikz}(\frac{1}{\rho}-\frac{1}{\rho_0}\frac{I_1(k\rho_0)(I_0(k\rho)-\frac{1}{k\rho}I_1(k\rho))}{I_1(k\rho)(I_0(k\rho_0)-\frac{1}{k\rho_0}I_1(k\rho_0))})$$

$$\times \quad \frac{g(k)}{k^2}dk, \tag{A.6}$$

$$E_\phi(\rho,\phi,z) = -i\omega G_x\rho\sin\phi\frac{1}{2\pi}\int_{-\infty}^{\infty} e^{ikz}\frac{g(k)}{k}(\frac{(I_0(k\rho)-\frac{1}{k\rho}I_1(k\rho))}{I_1(k\rho)}$$

$$- \quad \frac{I_1(k\rho_0)}{k^2\rho\rho_0(I_0(k\rho)-\frac{1}{k\rho}I_1(k\rho))})dk, \tag{A.7}$$

$$E_z(\rho,\phi,z) = \omega G_y\rho\cos\phi\frac{1}{2\pi}\int_{-\infty}^{\infty} e^{ikz}\frac{g(k)}{k}\frac{I_1(k\rho_0)}{k\rho_0(I_0(k\rho_0)-\frac{1}{k\rho_0}I_1(k\rho_0))}dk, \tag{A.8}$$

$$B_\rho(\rho,\phi,z) = \omega G_y\rho\sin\phi\frac{1}{2\pi}\int_{-\infty}^{\infty} e^{ikz}g(k)\frac{(I_0(k\rho)-\frac{1}{k\rho}I_1(k\rho))}{I_1(k\rho)}dk, \tag{A.9}$$

$$B_\phi(\rho,\phi,z) = -iG_y\cos\phi\frac{1}{2\pi}\int_{-\infty}^{\infty} e^{ikz}\frac{g(k)}{k}dk. \tag{A.10}$$

Using the small argument approximation of the modified Bessel's functions inside the equations, simplified expressions become:

$$E_\rho(\rho,\phi,z) = i\omega G_y\cos\phi(\frac{{\rho_0}^2-\rho^2}{4}), \tag{A.11}$$

$$E_\phi(\rho,\phi,z) = -i\omega G_y\sin\phi(\frac{{\rho_0}^2+\rho^2}{4}), \tag{A.12}$$

$$E_z(\rho,\phi,z) = i\omega G_y\rho z\cos\phi, \tag{A.13}$$

$$B_\rho(\rho,\phi,z) = G_y z\sin\phi, \tag{A.14}$$

$$B_\phi(\rho,\phi,z) = G_y z\cos\phi. \tag{A.15}$$

APPENDIX B

Simplification of the Electric Field Expressions for z-gradient coil

For z-gradient coil, target field is $B_z(\rho,\phi,z) = G_z z g(z)$ and the relation between J_ϕ^m and B_z^m is $J_\phi^m(k) = -\frac{G_z \delta(m) \int e^{-ikz} g(z) z dz}{\mu_0 k a I_m(k\rho) K'_m(ka)}$. According to that, fields become:

$$\begin{aligned}
E_\rho(\rho,\phi,z) &= i\omega G_z \frac{1}{2\pi} \sum_{m=-\infty}^{\infty} e^{im\phi} \int_{-\infty}^{\infty} e^{ikz} \frac{m\delta(m) \int e^{-ikz} g(z) z dz}{k^2} \\
&\times \left(\frac{1}{\rho} - \frac{I_m(k\rho_0) I'_m(k\rho)}{\rho_0 I_m(k\rho) I'_m(k\rho_0)}\right) dk, \qquad \text{(B.1)} \\
E_\phi(\rho,\phi,z) &= -i\omega G_z \frac{1}{2\pi} \sum_{m=-\infty}^{\infty} e^{im\phi} \int_{-\infty}^{\infty} e^{ikz} \frac{\delta(m) \int e^{-ikz} g(z) z dz}{k} \\
&\times \left(\frac{I'_m(k\rho)}{I_m(k\rho)} - \frac{m^2 I_m(k\rho_0)}{k^2 \rho \rho_0 I'_m(k\rho_0)}\right) dk, \qquad \text{(B.2)} \\
E_z(\rho,\phi,z) &= i\omega G_z \frac{1}{2\pi} \sum_{m=-\infty}^{\infty} e^{im\phi} \int_{-\infty}^{\infty} e^{ikz} \frac{m\delta(m) \int e^{-ikz} g(z) z dz}{k^2 \rho_0} \\
&\times \frac{I_m(k\rho_0)}{I'_m(k\rho_0)} dk, \qquad \text{(B.3)} \\
B_\rho(\rho,\phi,z) &= -iG_z \frac{1}{2\pi} \sum_{m=-\infty}^{\infty} e^{im\phi} \int_{-\infty}^{\infty} e^{ikz} \frac{\delta(m) \int e^{-ikz} g(z) z dz}{I_m(k\rho)} \\
&\times I'_m(k\rho) dk, \qquad \text{(B.4)}
\end{aligned}$$

$$B_\phi(\rho,\phi,z) = G_z\frac{1}{2\pi}\sum_{m=-\infty}^{\infty} e^{im\phi}\int_{-\infty}^{\infty} e^{ikz}\frac{m\delta(m)\int e^{-ikz}g(z)zdz}{k\rho}dk. \quad \text{(B.5)}$$

For this case, due to $\delta(m)$ function, the summation indices become $m = 0$. By using recurrence relations for Bessel's functions and the small argument approximation of the modified Bessel's functions given in Chapter 3 inside the equations, simplified expressions become:

$$E_\rho(\rho,\phi,z) = 0, \quad \text{(B.6)}$$

$$E_\phi(\rho,\phi,z) = -i\omega G_z\frac{\rho}{2}z, \quad \text{(B.7)}$$

$$E_z(\rho,\phi,z) = 0, \quad \text{(B.8)}$$

$$B_\rho(\rho,\phi,z) = -G_z\frac{\rho}{2}, \quad \text{(B.9)}$$

$$B_\phi(\rho,\phi,z) = 0. \quad \text{(B.10)}$$

Bibliography

[1] R. Bowtell and R. Bowley, "Analytic calculations of the E-fields induced by time varying magnetic fields generated by cylindrical gradient coils," *Magn Reson Med*, vol. 44, pp. 782–790, 2000.

[2] J. P. Reilly and A. M. Diamant, "Theoretical evaluation of peripheral nerve stimulation during MRI with an implanted spinal fusion stimulator," *Magn. Res. Imag.*, vol. 15, no. 10, pp. 1145–1156, 1997.

[3] J. Webster, *Wiley Encyclopedia of Electrical and Electronics Engineering*. John Wiley and Sons Inc., 1999.

[4] F. G. Shellock, "Magnetic resonance safety update 2002: Implants and devices," *J Magn Reson Imaging*, vol. 16, pp. 485–496, 2002.

[5] A. Roguin, M. Zviman, G. R. Meininger, E. R. Rodrigues, D. A. B. Timm M. Dickfeld, A. Lardo, R. D. Berger, H. Calkins, and H. R. Halperin, "Modern pacemaker and implantable cardioverter/defibrillator systems can be magnetic resonance imaging safe: In vitro and in vivo assessment of safety and function at 1.5 T," *Circulation*, vol. 110, pp. 475–482, 2004.

[6] D. Formica and S. Silvestri, "Biological effects of exposure to magnetic resonance imaging: an overview," *BioMedical Engineering OnLine*, vol. 3, no. 11, 2004.

[7] A. Kangarlu and P.-M. L. Robitaille, "Biological effects and health implications in magnetic resonance imaging," *Concepts in Magnetic Resonance,*, vol. 12, no. 5, pp. 321–359, 2000.

[8] F. G. Shellock, *Reference Manual for Magnetic Resonance Safety, Implants, and Devices*. Biomedical Research Publishing Group, 2007.

[9] J. Nyenhuis, "Interactions of medical implants with the magnetic fields in MRI," *The 25" Annual lntemational Conference of the IEEE EMBS*, 2003.

[10] R. Luechinger, "In vivo heating of pacemaker leads during magnetic resonance imaging," *Eur Heart J*, vol. 26, pp. 376–383, 2005.

[11] H. Irak, "Modelling RF heating of implantable medical devices during MRI using safety index," 2007.

[12] H. Siebold, "Design optimization of main, gradient and RF field coils for MR imaging," *IEEE on Magn.*, vol. 26, no. 2, pp. 841–846, 1990.

[13] B. A. Chronik, "Peripheral nerve stimulation in MRI gradient coils," *ISMRM Berlin*, 2007.

[14] B. A. Chronik and B. K. Rutt, "A comparison between human magnetostimulation thresholds in whole-body and head/neck gradient coils," *Magn Reson Med*, vol. 46, pp. 386–384, 2001.

[15] F. M. Vogt, M. E. Ladd, P. Hunold, S. Mateiescu, F. X. Hebrank, A. Zhang, J. F. Debatin, and S. C. Göhde, "Increased time rate of change of gradient fields: Effect on peripheral nerve stimulation at clinical MR imaging," *Radiology*, vol. 233, no. 2, pp. 548–554, 2004.

[16] B. Zhang, Y.-F. Yen, B. A. Chronik, G. C. McKinnon, D. J. Schaefer, and B. K. Rutt, "Peripheral nerve stimulation properties of head and body gradient coils of various sizes," *Magn Reson Med*, vol. 50, pp. 50–58, 2003.

[17] B. A. Chronik and M. Ramachandran, "Simple anatomical measurements do not correlate significantly to individual peripheral nerve stimulation thresholds as measured in MRI gradient coils," *Magn Reson Med*, vol. 17, pp. 716–321, 2003.

[18] A. Hoffmann, S. Faber, K. Werhahn, L. Jager, and M. Reiser, "Electromyography in MRI first recordings of peripheral nerve activation caused by fast magnetic field gradients," *Magn Reson Med*, vol. 43, pp. 534–539, 2000.

[19] a. K. E. J. Abart, H. Fischer, W. Huk, E. Richter, F. Schmitt, T. Storch, and E. Zeitler, "Peripheral nerve stimulation by time-varying magnetic fields," *J. Comput. Assist. Tomogr.*, vol. 21, pp. 532–538, 1997.

[20] H. Zhao, S. Crozier, , and F. Liu, "Finite difference time domain (FDTD) method for modeling the effect of switched gradients on the human body in MRI," *Magn Reson Med*, vol. 48, pp. 1037–1042, 2002.

[21] P. So, K. Caputa, and M. A. Stuchly, "Peripheral nerve stimulation by gradient switching fields in MRI," *Proceedings of the 25' Annual lntematianal Conference of the IEEE EMBS*, 2003.

[22] D. Buechler, C. Durney, and D. Christensen, "Calculation of electric fields induced near metal implants by magnetic resonance imaging switched gradient magnetic fields," *Magn. Res. Imag.*, vol. 15, no. 10, pp. 1157–1166,, 1997.

[23] W. Irnich, B. Irnich, C. Bartsch, W. A. Stertmann, H. Gufler, and G. Weiler, "Do we need pacemakers resistant to magnetic resonance imaging?," *Europace*, vol. 7, pp. 353–365, 2005.

[24] J. M. B. Kroot, *Analysis of Eddy Currents in a Gradient Coil*. PhD thesis, Technische Universiteit Eindhoven, 2005.

[25] H. Siebold, "Gradient field coils for MR imaging with high spectral purity," *IEEE on Magn.*, vol. 26, no. 2, pp. 897–900, 1990.

[26] J. Jin, *Electromagnetic Analysis and Design in Magnetic Resonance Imaging*. CRC Press LLC, 1999.

[27] M. A. Bernstein, X. J. Zhou, J. A. Polzin, K. F. King, A. Ganin, N. J. Pelc, and G. H. Glover, "Concomitant gradient terms in phase contrast MR: Analysis and correction," *Magn Reson Med*, vol. 39, pp. 300–308, 1998.

[28] R. Turner, "Gradient coil design: A review of methods," *Magn. Res. Imag*, vol. 11, pp. 903–920, 1993.

[29] M. A. Brideson, L. K. Forbes, and S. Crozier, "Determining complicated winding patterns for shim coils using stream functions and the target-field method," *Concepts in Magnetic Resonance*, vol. 14, pp. 9–18, 2002.

[30] R. Turner, "A target field approach to optimal coil design," *Magn. Res. Imag.*, vol. 19, pp. L147–L151, 1986.

[31] N. G. Gençer and M. N. Tek, "Imaging tissue conductivity via contactless measurements: A feasibility study," *ELEKTRIK*, vol. 6, no. 3, pp. 183–200, 1998.

[32] J. A. Kong, *Electromagnetic Wave Theory*. John Wiley and Sons, 1986.

[33] R. Turner and R. M. Bowley, "Passive screening of switched magnetic field gradients," *J. Phys. E: Sci. Instrum.*, vol. 19, no. 10, pp. 876–879, 1986.

[34] M. Abramowitz and I. A. Stegun, *Handbook of Mathematical Functions*. New York: Dover, 1965.

[35] E. Abacı, E. Kopanoğlu, V. B. Ertürk, and E. Atalar, "Simple analytical equation of the induced E-field," *ISMRM Toronto*, 2008.

[36] W. A. Tacker and L. A. Geddes, "The laws of electrical stimulation of cardiac tissue," *IEEE*, vol. 84, no. 3, pp. 355–365, 1996.

[37] D. Schaefer, J. Bourland, and J. Nyenhuis, "Review of patient safety in time-varying gradient fields," *J Magn Reson Imaging*, vol. 12, pp. 20–29, 2000.

[38] IEC, *Particular requirements for basic safety and essential performance of magnetic resonance equipment for medical diagnosis*. IEC Std. 62B/669/CD, 2007.

[39] J. P. Reilly, "Magnetic field excitation of peripheral nerves and the heart: a comparison of thresholds," *Med. and Biol. Eng. and Comput.*, vol. 29, pp. 571–579, 1991.

[40] F. G. Shellock, L. Fischer, and D. S. Fieno, "Cardiac pacemakers and implantable cardioverter defibrillators: In vitro magnetic resonance imaging evaluation at 1.5-Tesla," *Journal of Cardiovascular Magnetic Resonance*, vol. 9, pp. 21–31, 2007.